9-15-2015 12:00 AM

Effect of Hemiarthroplasty Implant Contact Geometry and Material on Early Cartilage Wear

Alana Khayat
The University of Western Ontario

Supervisor
Dr. James Johnson
The University of Western Ontario

Graduate Program in Biomedical Engineering
A thesis submitted in partial fulfillment of the requirements for the degree in Master of Engineering Science

Effect of Hemiarthroplasty Implant Contact Geometry and Material on Early Cartilage Wear

Thesis format: Integrated Article

by

Alana Khayat

Graduate Program in Biomedical Engineering
A thesis submitted in partial fulfillment
of the requirements for the degree of
Master of Engineering Science

The School of Graduate and Postdoctoral Studies
The University of Western Ontario
London, Ontario, Canada

Abstract

Hemiarthroplasty is a minimally invasive, cost-effective alternative to total arthroplasty in joints of the upper limb. Though these procedures reduce patient morbidity while restoring joint kinematics, their longevity is limited by wear of the adjacent cartilage. This work investigates the roles of contact geometry and implant stiffness on cartilage wear with the aim of elucidating the mechanics that contribute to cartilage damage. An *in vitro* study examined the influence of implant geometry on cartilage wear using a pin-on-plate wear simulator. A significant decrease in volumetric wear was observed as contact area increased, which suggests that maximizing contact area should be a design target for hemiarthroplasty implants. A subsequent study examined the influence of stiffness using various clinically relevant biomaterials, and demonstrated no effect on cartilage wear for a range of Young's moduli between 200 GPa and 0.69 GPa. It was concluded that the disparity between the moduli of the investigated materials and that of cartilage may be too great to demonstrate the possible effects of implant stiffness on contact mechanics. A finite element simulation was conducted to further reveal contact mechanics at the implant-cartilage interface. The stress levels determined by the study were proportional to the wear in both *in vitro* studies conducted, with the exception of polyether ether ketone, one of the investigated biomaterials. Further studies are required to more comprehensively characterize cartilage wear, and it is necessary to examine whether stiffness has an effect on cartilage wear when caused by implant materials with moduli approaching that of articular cartilage.

Keywords

Hemiarthroplasty, cartilage wear, biomechanics, elbow, shoulder, contact area, Young’s modulus, biomaterials

Co-Authorship Statement

Chapter One–sole authorship

Chapter Two

Study Design- Alana Khayat, Dan Langohr, John Medley, Graham King, Jim Johnson
Data Gathering-Alana Khayat
Data Analysis- Alana Khayat, Ryan Willing
Technical Oversight- Dan Langohr
Statistical Analysis- Alana Khayat
Writing- Alana Khayat
Revisions- Alana Khayat, John Medley, Graham King, Jim Johnson

Chapter Three

Study Design- Alana Khayat, Dan Langohr, John Medley, Graham King, Jim Johnson
Data Gathering-Alana Khayat
Data Analysis- Alana Khayat, Ryan Willing
Technical Oversight- Dan Langohr
Statistical Analysis- Alana Khayat
Writing- Alana Khayat
Revisions- Alana Khayat, John Medley, Graham King, Jim Johnson

Chapter Four

Study Design- Alana Khayat, Dan Langohr
Model Construction-Alana Khayat, Dan Langohr
Data Gathering-Alana Khayat
Data Analysis- Alana Khayat
Technical Oversight- Dan Langohr
Statistical Analysis- Alana Khayat
Writing- Alana Khayat
Revisions- Alana Khayat, John Medley, Graham King, Jim Johnson

Chapter Five – sole authorship

Appendix A – sole authorship

Appendix B

Study Design- Alana Khayat, Dan Langohr, Graham King, Jim Johnson
Data Gathering-Alana Khayat

Data Analysis- Alana Khayat
Statistical Analysis- Alana Khayat

Appendix C

Study Design- Alana Khayat, Dan Langohr, Jim Johnson
Data Gathering-Alana Khayat
Data Analysis- Alana Khayat

Appendix D

Study Design- Alana Khayat, Dan Langohr, Jim Johnson
Data Gathering-Alana Khayat
Data Analysis- Alana Khayat

Appendix F

Study Design- Alana Khayat, Dan Langohr, Jim Johnson
Data Gathering-Alana Khayat
Data Analysis- Alana Khayat

Appendix G

Study Design- Alana Khayat, Dan Langohr, Jim Johnson
Data Gathering-Alana Khayat
Data Analysis- Alana Khayat

Appendix H

Study Design- Alana Khayat, Dan Langohr, Jim Johnson
Data Gathering-Alana Khayat
Data Analysis- Alana Khayat, Emily Lalone, Ryan Willing

Appendix I

Study Design- Alana Khayat, Dan Langohr, Jim Johnson
Data Gathering-Alana Khayat
Data Analysis- Alana Khayat

Acknowledgments

First and foremost, I thank my supervisor Dr. James Johnson, without whom none of this work would have been possible. Dr. Johnson is endlessly curious, engaged, and showed infinite patience and grace throughout this process where mine often wore thin. Bringing humour and lightness to this process is almost as impressive a feat as his many academic and professional accomplishments. Along the same lines, Dr. Graham King provided consistently striking insights and advice while remaining ever grounded and reasonable. Working with such a staggeringly impressive scientist and surgeon was truly inspirational, especially because Dr. King is such a joy.

Dr. John Medley, who has encyclopedic knowledge of all things wear related and stronger convictions than anyone I've ever met, was an invaluable resource. The meticulousness with which he approaches research and the decisiveness with which he evaluates studies is unparalleled, and this sort of passion for scientific integrity is so admirable. His critiques and commentary were incredibly constructive and educational.

Dan Langohr provided more direct support (conceptual and technical), council, and guidance than I can adequately express. Dan thoughtfully answered every little question I had and was always so generous with his time. His brilliance is only matched by his humility, which made him the best mentor of which I can conceive. To the rest of the HULC students, thank you so much for the fun times and interesting (if sorted) lunch conversation and conference trips; working with such a competent, well-rounded group of people was really motivating.

Finally, I'd like to thank my parents for their infinite love and encouragement though all of the ups and down of the past two years, of which there were many. I carry you with me everywhere I go.

Table of Contents

Abstract i

Co-Authorship Statement ii

Acknowledgments iv

Table of Contents v

List of Tables ix

List of Figures x

List of Appendices xii

List of Abbreviations xiii

Chapter 1 1

Hemiarthroplasty in the Upper Limb: Indications and Complications 1

1.1 The Mechanical Function of Articular Cartilage 1

1.2 Shoulder and Elbow Anatomy, Function, and Mechanics 3

1.3 Hemiarthroplasty in the upper limb: Indication, Incidence, and Issues 6

1.4 Cartilage Wear 8

1.4.1 Quantification of Cartilage Wear 8

1.5 Finite Element Modeling of Hemiarthroplasty Implants Against Cartilage 12

1.6 Rationale 14

1.7 Objectives and Hypotheses 15

1.7.1 Objectives 15

1.7.2 Hypotheses 15

1.8 Thesis Overview 16

1.9 References 17

Chapter 2 30

2 The Effect of Hemiarthroplasty Implant Geometry on Early *In Vitro* Cartilage Wear 30
2.1 Introduction 30
2.2 Materials and Methods 32
2.2.1 Tissue Acquisition and Preparation 32
2.2.2 Tribological Simulation 33
2.2.3 Wear Quantification 35
2.3 Results 36
2.4 Discussion 39
2.5 Conclusions 44
2.6 References 45
Chapter 3 50
3 The Effect of Hemiarthroplasty Implant Material on Early *In Vitro* Cartilage Wear .. 50
3.1 Introduction 50
3.2 Materials and Methods 52
3.2.1 Implant models 52
3.2.2 Tissue Acquisition and Preparation 53
3.2.3 Tribological Simulation 53
3.2.4 Wear Assessment 55
3.3 Results 55
3.3.1 Volumetric Wear 55
3.3.2 Scanning Electron Microscopy 57
3.4 Discussion 58
3.5 Conclusion 61
3.6 References 62
Chapter 4 66

4 The Effect of Hemiarthroplasty Implant Geometry and Material on Contact Mechanics: A Finite Element Analysis 66

4.1 Introduction 66

4.2 Materials and Methods 67

4.2.1 Implant Models 67

4.2.2 Cartilage and Bone Models 68

4.2.3 Boundary and Loading Conditions 69

4.2.4 Measurement Regions and Output Variables 70

4.2.5 Model Validation 70

4.3 Results 71

4.4 Discussion 74

4.5 Conclusion 78

4.6 References 79

Chapter 5 83

5 Overall Conclusions and Future Research Directions 83

5.1 Three Dimensional Scanning Protocol for the Measurement of Cartilage Wear 83

5.2 The Effect of Implant Contact Radius on Cartilage Wear 84

5.3 The Effect of Implant Stiffness on Cartilage Wear 85

5.4 The Effect of Implant Stiffness Contact Geometry and Stiffness on Cartilage Contact Mechanics: A Finite Element Study 85

5.5 Conclusion 86

Appendices 87

Appendix A- Glossary 87

Appendix B- The Effect of Freezing on the Mechanical Properties of Articular Cartilage 89

Appendix C- Volumetric Wear of a Hemiarthroplasty Implant Roughness Grade Material 91

Appendix D- The Time-Dependence of Cartilage Wear 92

Appendix E- Determination of Applied Load Level 94

Appendix F- Comparison of Clinical Contact Stresses and Contact Stresses of all Investigated Implant Models 96

Appendix G- Cartilage Creep Measurements for all Testing Configurations implant models 97

Appendix H- MeshLab Mesh Registration, VTK Inter-Mesh Distance Algorithm, and MATLAB Volume Calculation Protocols 98

Appendix I- Contact Area Measurements for Various Measurement Techniques 101

Curriculim Vitae 102

List of Tables

Table 3-1 Implant Material Properties 52

Table 4-1 Implant Material Properties 68

Table 4-2 Summary of FEA Results for Varying Implant Geometry 72

Table 4-3 Summary of FEA Results for Varying Material 73

Table A-1 Surface roughness measurements and volumetric wear for implant materials . 91

Table A-2 Variables used in Hertizian Contact Stress Calculation 94

Table A-3 Average contact stresses for implant models 95

Table A-4 Clinically Measured Contact Stresses for Various Hemiarthroplasty Procedures 95

Table A-5 Penetration depth and recovery time for cartilage loaded statically 96

Table A-6 Contact area measurements for various techniques 100

List of Figures

Figure 1-1Biphasic contact between cartilage surfaces 1

Figure 1-2 The anatomy of the elbow and forearm 5

Figure 1-3 The bony anatomy of the shoulder. 6

Figure 1-4 A common hemiarthroplasty procedure in the upper limb: radial head replacement. 7

Figure 2-1 Implant models with radii of curvature. E=200 GPa, ν=0.28. 32

Figure 2-2 Pin-on-disk wear simulator loading configuration 34

Figure 2-3 a) Scan of unworn cartilage surface b) Scan of worn cartilage surface c) Colour-contour map showing distance between worn and unworn surfaces. 36

Figure 2-4 Volumetric wear caused by each implant model shown as a function of implant radius of curvature 37

Figure 2-5 Average wear depth caused by each implant mode shown as a function of implant radius of curvature 38

Figure 2-6 India ink stains of cartilage specimens in order of increasing radius of curvature 39

Figure 2-7 Wear behaviour at different ranges of radius of curvature 40

Figure 3-1 Pin-on-disk wear simulator loading configuration 54

Figure 3-2 Average volumetric wear for each implant material 56

Figure 3-3 Comparison of India ink stains. 57

Figure 3-4 SEM Images of an implant of each material taken at 10kV electron beam energy. 58

Figure 4-1 Implant geometries modeled 67

Figure 4-2 Implant models, in order of descending Young's Modulus. 68

Figure 4-3 Boundary conditions and meshes for finite element models. 69

Figure 4-4 Comparison of contact area measurements from casting, pressure-sensitive film, and finite element analysis for the ROC=5.10mm implant model..... 71

Figure 4-5 Summary of FEA Resultsfor varying implant geometry 72

Figure 4-6 Von Mises Stress distributions along implant-cartilage interface in order of increasing radius of curvature. 73

Figure 4-7 Summary of FEA Results for varying implant material 74

Figure 4-8 a) FEA Peak von Mises Stress as a Function of radius of curvature(ROC) with slopes between segments shown. b) Average volumetric wear results as a function of radius of curvature.. 76

Figure A-1Percent area damage for fresh and frozen cartilage specimens. 90

Figure A-2 Volumetric wear for various materials, in order of ascending surface roughness average measurement..... 89

Figure A-3 Volumetric wear as a function of number of reciprocation cycles..... 90

Figure A-4 Penetration depth of a 4.70 mm radius of curvature hemispherical tip pin under a constant, static load of 27.5 N as a function of time..... 95

Figure A-5.m file to compute volume between worn and unworn surface meshes..... 96

List of Appendices

Appendix A- Glossary 87

Appendix B- The Effect of Freezing on the Mechanical Properties of Articular Cartilage 89

Appendix C- Volumetric Wear of a Hemiarthroplasty Implant Roughness Grade Material 91

Appendix D- The Time-Dependence of Cartilage Wear 92

Appendix E- Determination of Applied Load Level 94

Appendix F- Comparison of Clinical Contact Stresses and Contact Stresses of all Investigated Implant Models 96

Appendix G- Cartilage Creep Measurements for all Testing Configurations implant models 97

Appendix H- MeshLab Mesh Registration, VTK Inter-Mesh Distance Algorithm, and MATLAB Volume Calculation Protocols 98

Appendix I- Contact Area Measurements for Various Measurement Techniques 101

List of Abbreviations

ACS	Alpha calf serum
Al_2O_3	Alumina
CoCr	Cobalt chromium
FEA	Finite element analysis
FES	Finite element simulation
HDPE	High density polyethylene
NMR	Nuclear magnetic resonance
PBS	Phosphate-buffered saline
PEEK	Polyether ether ketone
PU	Polyurethane
ROC	Radius of curvature
SEM	Scanning electron microscopy
Si_3N_4	Silicon nitride
SS	Stainless steel
Ti	Titanium
UHMWPE	Ultra high molecular weight polyethylene

Chapter 1

Hemiarthroplasty in the Upper Limb: Indications and Complications

1.1 The Mechanical Function of Articular Cartilage

The primary function of articular, or hyaline, cartilage is to provide bearing surfaces in synovial joints. The synovial joint permits relative motion of the surfaces with low friction while transmitting high forces without damage to its structural components. By virtue of its compliance and multiphasic composition, cartilage reduces articular stresses, both within itself and in the supporting subchondral bone[1-4]. While cartilage is usually modeled as a biphasic material consisting of solid and liquid phases, negative ions in one of its constituents also have an effect on its mechanical properties[1]. Figure 1-1 shows the way in which low global contact pressures are maintained in biphasic contact within synovial joints[5].

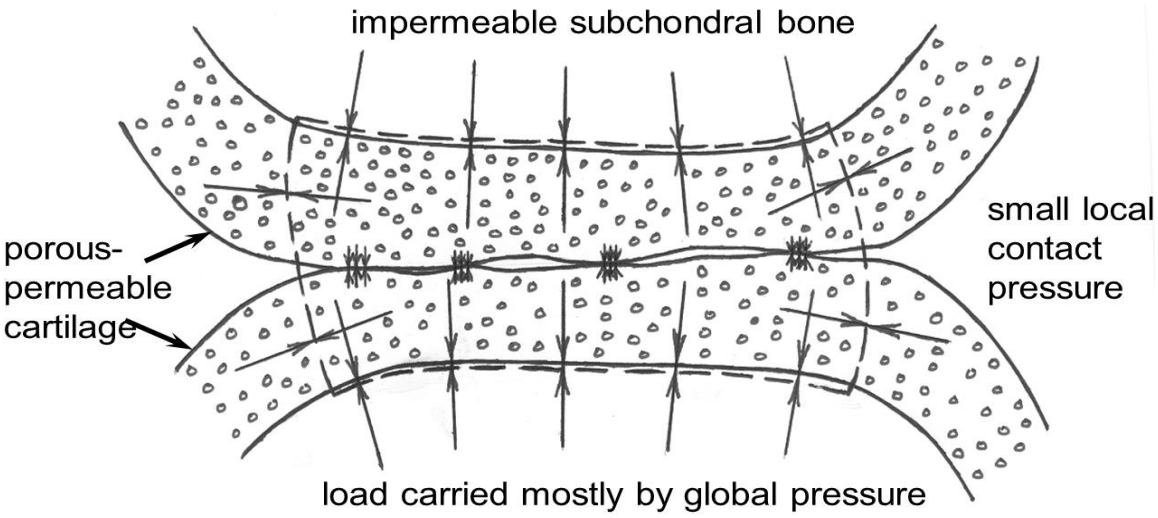

Figure 1-1 *Biphasic contact between cartilage surfaces reduces the incidence of stress concentrations and reduces contact pressure by increasing articular contact area. The small arrows at the articulation represent small, local contact areas. (ME 598 Engineering Biomechanics lecture notes, reproduced with permission of Professor JB Medley, Department of Mechanical and Mechatronics Engineering, University of Waterloo)*

Most of cartilage's constitution, between 70 and 85 %, is aqueous, and rest consists of proteoglycans and collagen. Proteoglycans have a protein core onto which chondrotin sulfate and keratan sulfate bind to make a 'bottlebrush-like' structure, and account for 30% of cartilage's dry weight[4]. The rest of the solid phase is made of collagen, which is the most prevalent structural protein from which animal connective tissues are made. Type II collagen is the primary constituent of cartilage's extracellular matrix. The living component of cartilage is composed of cells called chondrocytes, which are suspended throughout the collagen-proteoglycan matrix. The structure, distribution, and relative compositions of all these components varies with the proximity to the articular surface and subchondral bone as follows[4]:

1) The calcified region, which consists of tightly packed bundles of radially-oriented collagen.
2) The upper deep zone, which consists of the radiate and intermediate zones, in which the orientation of the collagen becomes less distinct. This layer forms the matrix in which chondrocytes are suspended.
3) The superficial zone, in which finer fibers are arranged into layers.
4) The articular surface, an amorphous layer that is relatively smooth, though its actual surface roughness during loaded, sliding motion is unknown.

Confined compression and indentation tests are typically used to measure the material properties of cartilage *in vitro* and *in situ* respectively, although some testing of whole joints under *in vivo* conditions has been performed. From compression tests, the aggregate modulus of cartilage is in the range of 0.5 to 0.9 MPa and the Young's modulus ranges between 0.45 and 0.8 MPa[4,6] although some studies quote a higher value of 1.79 MPa for Young's modulus[7]. Interestingly, an early study that examined the cyclic steady state response of articular cartilage to sinusoidal loading measured compressive Young's moduli in the range of 12 to 50 MPa[8]. Permeability, which is a material's resistance to fluid flow, can also be determined in cartilage using these tests. While permeability varies throughout the aforementioned layers, it is also related to compressive loading; when a joint is loaded, the fluid flow out of the cartilage matrix will decrease[9]. Indentation tests

have demonstrated that the Poisson's ratio of cartilage is usually less than 0.4 and often approaches zero[1,2]. The frictional coefficient of cartilage against itself has also been shown to vary with loading; in dynamic loading, it is very low, between 0.002-0.02, but upon static loading, it increases to 0.2-0.4 over a period of several hours[10].

Throughout joint motion, cartilage is subjected to repeated loading, friction, and traumatic injury, all of which can contribute to its degeneration, though maintenance of joint contact stresses is important for the regeneration of cartilage and bone. Acute, trauma-induced cartilage damage may heal depending on wound depth, but since cartilage does not have a direct blood supply, its capacity to repair itself is limited. Local cartilage defects caused by mechanical impacts like falls or direct blows may also release fragments of cartilage and bone chips into the joint capsule, which interfere with joint motion. Cartilage is also vulnerable to more progressive mechanical degeneration caused by 'wear and tear.' Like in any material, fatigue leads to the progressive degeneration of cartilage, the rate of which depends on a number of factors including age and activity level[4]. Cartilage softening, which often begets this sort of damage, progresses to fissuring, fragmentation, and thinning that may eventually expose subchondral bone.

Regardless of the mechanism of injury, cartilage damage contributes to osteoarthritis, a painful, degenerative disease that presents as joint pain, swelling, decreased range of motion, and, in cases where fragmentation has occurred, 'locking' during joint motion. This mechanically-driven process results in a decrease in the cartilage's Young's modulus and an increase in permeability. These changes compromise cartilage's ability to bear loads, to produce chondrocytes, and to facilitate smooth, painless motion [4]. Reactive bone formation, or eburnation, in which an unhealthy increase in bone density at the site of cartilage erosion,is also common[6].

1.2 Shoulder and Elbow Anatomy, Function, and Mechanics

Proper function of the joints of the upper limb is critical to the maintenance of physical independence. The joints of the elbow and shoulder enable a wide range of motion, the reduction of which make activities of daily living including feeding, dressing, and grooming oneself very difficult[11]. The elbow connects the bones of the forearm, the

radius and the ulna, to the arm bone, the humerus. It consists of three joints which come together to effectively transmit forces between the shoulder and the wrist, as well as to increase the precision of hand placement[12] .The elbow's notable stability can be attributed to the "tongue and groove" configuration of the ulnohumeral joint, whereas the elbow's wide range of motion can be attributed to the articulation between the spherical capitellum and the concave surface of the radial head[13-15]. The third joint of the elbow is the proximal radioulnar joint, which allows the radius to rotate about the ulna's axis during forearm rotation. Elbow joint anatomy and motions are illustrated in Figure 1-2. If the structural integrity of one of the elbow's components is compromised, its overall mobility and stability diminish.

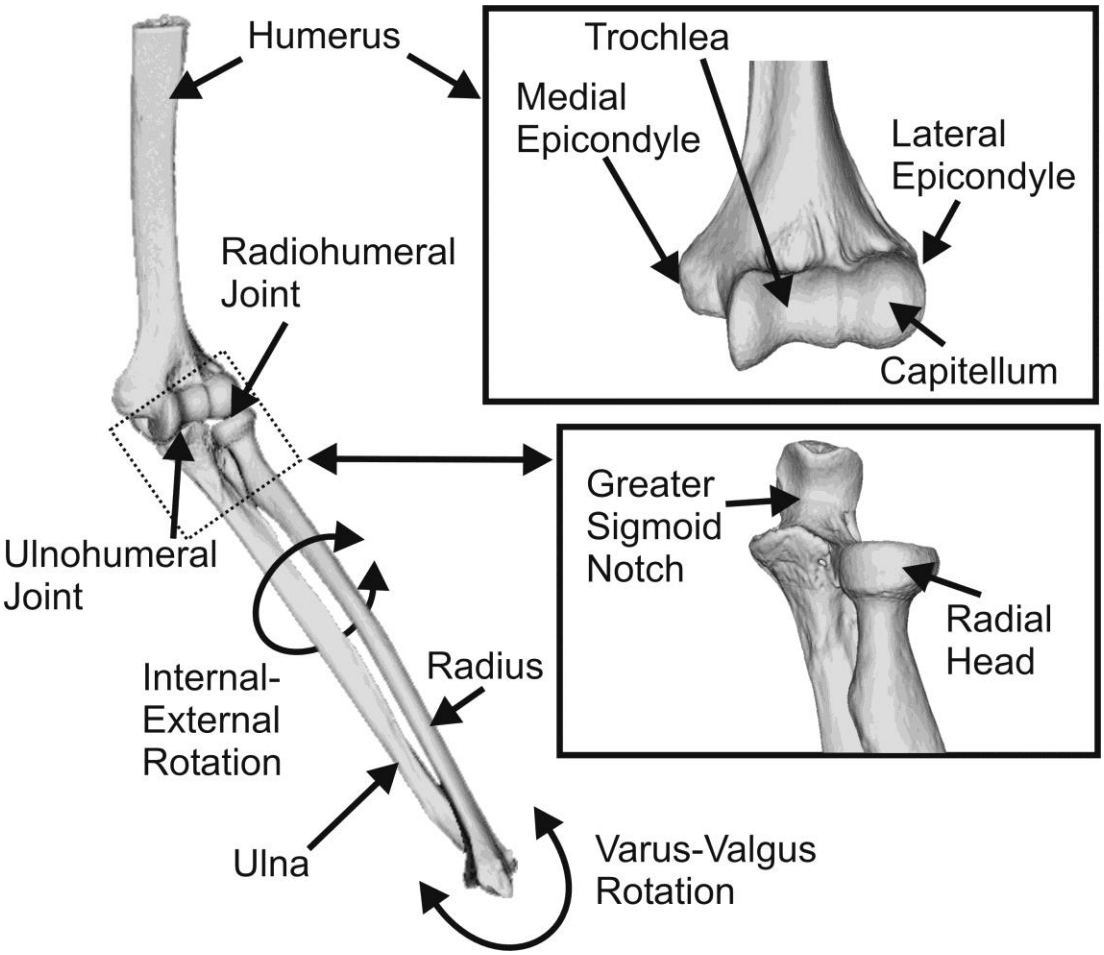

Figure 1-2 *The anatomy of the elbow and forearm. The joints of the elbow are the radiohumeral joint, ulnohumeral joint, and the proximal radioular joint. During flexion of the elbow, both varus-valgus rotation and internal-external rotations can occur.*

Like in the elbow, the shoulder unifies three bones to form three individual joints[16]. However, the shoulder, shown in Figure 1-3, is a comparably unstable joint and more prone to dislocation than the elbow. The glenohumeral joint, at which the spherical head of the humerus articulates with the glenoid, a shallow, dish-shaped groove in the scapula, accounts for most shoulder joint motion. The clavicle (or collar bone) articulates with the scapula at the upper part of the joint. These articulations form a ball-in-socket joint that has the largest range of motion of any joint in the body[17-20].

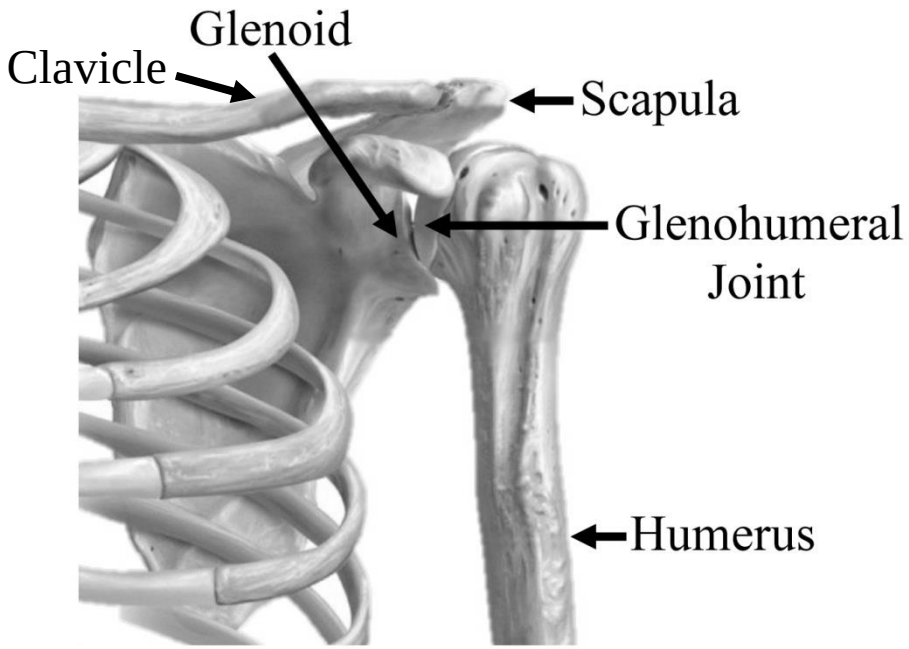

Figure 1-3 *The bony anatomy of the shoulder. The glenohumeral joint is shown, which makes the greatest contribution to the range of motion of the shoulder.*

1.3 Hemiarthroplasty in the upper limb: Indication, Incidence, and Issues

The complication and failure rates of total arthroplasty in the joints of the upper limb are higher than in the lower limbs, which may be attributed, in part, to the invasive surgical approach required for their implantation as well as to suboptimal prosthesis design[21-23]. Hemiarthroplasty, wherein only one of a joint's articulating surfaces is replaced, is less surgically invasive and constraining to postoperative motion than total arthroplasty[24]and maximizes the preservation of healthy tissue [25,26]. However, the interaction between these implants and native articular cartilage has the potential to be problematic. For this reason, particularly in the shoulder, total joint arthroplasty is more common, despite the invasiveness of the surgical implantation.

In the elbow, total joint arthroplasty can be employed in the event of injures such as distal humeral fractures, as well as for those suffering from degenerative cartilage diseases like

osteoarthritis and rheumatoid arthritis. However, in cases like radial head fracture, where only one of the joint's articulating surfaces is damaged, a hemiarthroplasty procedure is often employed (Figure 1-4). This procedure involves excising the radial head and replacing it with an implant, which articulates with the native capitellum. *In vitro* biomechanical studies on metallic radial head implants have shown that these implants can restore elbow kinematics and stability to be similar to that of the native radial head [27-30], and clinical studies show promising outcomes for restoration of motion and function[24,28].

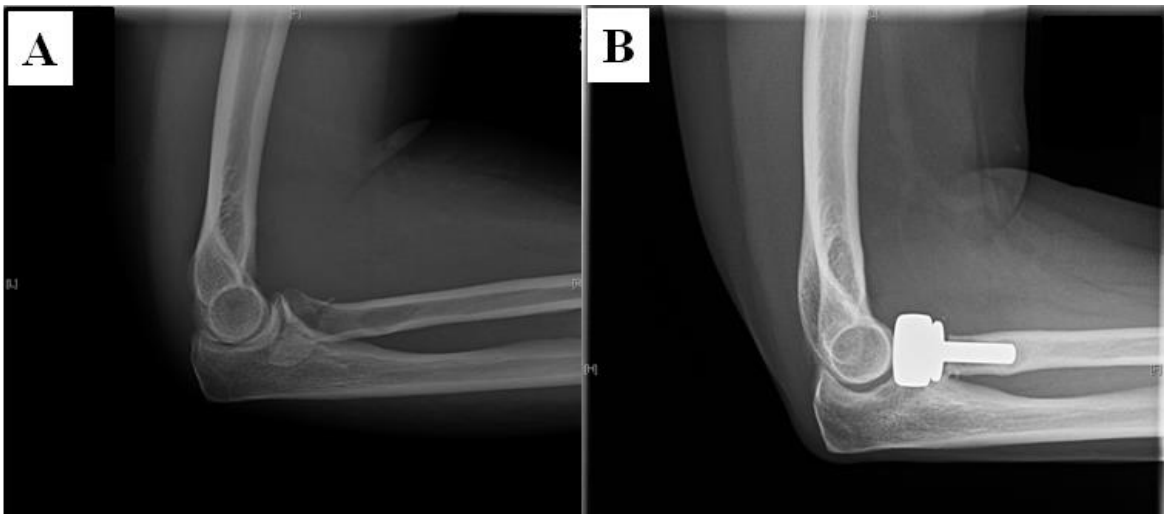

Figure 1-4*A common hemiarthroplasty procedure in the upper limb: radial head replacement. (A) Radiograph of a typical pre-operative comminuted radial head fracture in the right elbow; (B) Post-operative radiograph showing the implant which articulates against the humerus' capitellum.*

However, for these and other hemiarthroplasty-reconstructed joints, it has been suggested that the relatively high stiffness of metallic implants is problematic for long-term use due to the increased contact stresses and the wear of the articular cartilage adjacent to the implant that regularly ensues[24,31]. For example, a decrease in contact area of two thirds has been reported in metallic unipolar radial head implants, which results in greater contact pressures[32]. Joint areas subject to higher contact pressures are associated with increased cartilage degeneration[33]. Furthermore, increases in contact stress have been shown to promote the secretion of degenerative enzymes, which have a deteriorative effect on the

stiffness and elasticity of articular cartilage[34]. At the cellular level, compression injuries and fissuring have been associated with proteoglycan depletion as well as chondrocyte death[35-37].

Current replacements are typically non-anatomical in shape, hence they fail to maintain congruity with native bone. Combined with the increase in pressures acting though the joint, degenerative changes to the cartilage surface following the hemiarthroplasty procedure[31,38,39] have been shown to occur. This limits the longevity of hemiarthroplasty implants; furthermore, *in vivo* studies performed by Cruess et al. and Dalldorf et al. report a correlation between the severity of damage of articular cartilage and the length of time the implant is in place[55,94]. Similarly, Van Riet et al. detail the case of an 18 year old woman with preoperative healthy capitellar cartilage who underwent a radial head arthroplasty[40]. After 16 months, radiographs indicated that there was considerable wear on the side of the capitellum that articulated with the implant, where there was no wear to the ulnar side of the humerus. Furthermore, a 3mm misalignment in the patient's wrist was observed on the side that underwent the procedure. The authors attributed the capitellar erosion to the greater stiffness of the metal relative to native bone and the decreased radiocapitellar contact area.

Hemiarthroplasty is therefore primarily prescribed for relatively sedentary patients[24,41]. Since comminuted fractures of the radial head often occur in younger people[39] and shoulder hemiarthroplasty is commonly prescribed for young, athletic patients, current implants must be improved to increase the longevity and broaden the clinical applicability of these devices.

1.4 Cartilage Wear

1.4.1 Quantification of Cartilage Wear

Wear is defined as the removal of material from a surface as a result of a sliding interaction with another surface. The underlying mechanisms of wear include surface adhesion, abrasion, fatigue, and corrosion. While cartilage wear is difficult to quantify

because of its high water content, numerous studies have outlined *in vivo* and *in vitro* protocols to do so[10,42-49].

McGann et al. compared various *in vitro* methods of quantifying wear along with finite element analysis with the aim of establishing a methodology for screening implant materials and finishes[42]. This study utilized fresh-frozen bovine specimens that underwent two rounds of freezing and thawing throughout testing. Two different cartilage surface geometries were compared to determine the optimal testing configuration: smaller specimens with flat surfaces that made complete contact with the flat stainless steel counterface during wear testing, and larger, curved explants that made contact with the counterface in the center of the specimen but not at the edges.

Wear was quantified in three ways: the mass of collagen removed as a function of surface area, a semi-quantitative visual analysis, and by the change in surface roughness. The mass analysis was based on the principle that volumetric wear could be related to the protein content of the cartilage removed from the subchondral bone, which was collected from the lubricating bath after testing and measured using high performance liquid chromatography.

The mass analysis, which was taken to be the 'gold standard,' was compared to the other two methods to see if either could be a fast, accurate alternative. A number of studies have validated a visual method of quantifying wear using staining with India ink, which has been shown to adhere to fibrillated cartilage, and a computer pigment identification program[2,42]. The sort of fibrillation highlighted by the ink is a clear indicator of wear[43]. A study performed on cadaveric necropsy specimens utilized India ink staining to describe and classify the surface morphology, topography, and evolution of natural fibrillation in the articular cartilage[50], so it was suggested that a similar protocol could be used to quantify cartilage wear.

In the McGann et al. study, the visual analysis consisted of applying India ink to the surfaces of worn cartilage specimens[42]. The areas that remained stained after wiping the specimens with a damp cloth were identified as damaged based on India ink's adherence to fibrillated cartilage. The damage was assessed semi-quantitatively using Matlab pixel-

thresholding technology. The number of the stained pixels was counted and converted to an area, indicating the portion of the cartilage that was damaged. To account for the differences in contact areas among specimens, the stained contact area was normalized by to the total specimen area. The results of this semi-quantitative analysis correlated strongly with the results of their mass analysis. As such, this method was determined to be sufficiently precise and a sound alternative due to its executional ease and low cost[42].

Conversely, surface roughness, which was measured before and after testing, was deemed an inadequate metric for evaluating wear. The results did not correlate to the wear factor established by the mass analysis, though the general trend showed an increase of roughness after testing.

A similar methodology was used by Chan et al. to evaluate potential hemiarthroplasty materials[43]. Their tests consisted of wearing bovine cartilage with a pin-on-disk tribometer against alumina (Al_2O_3), cobalt chromium (CoCr), stainless steel (SS), and crosslinked ultra high molecular weight polyethylene (UHMWPE). Friction was measured by the tribometer and wear was quantified by the mass difference of the cartilage specimens. The mass of material removed from the surface was estimated by measuring the mass of the debris in the lubricating bath. Typically, mass wear is quantified using measurements of the dry mass of the worn material, but in this protocol, hydration was considered to be an important feature of cartilage. While no statistically significant differences were detected, the investigators highlighted trends that indicate that the CoCr- cartilage contact exhibited the least desirable tribological properties, and that UHMWPE had the best performance in terms of wear.

Lizhang et al. examined the effects of loading time, contact stress and area, sliding distance, and sliding speed on wear, with the specific aim of improving the outcomes of hip hemiarthroplasty[10]. Fresh-frozen bovine cartilage was worn using a pin-on-plate simulator that reciprocated flat cartilage plugs against CoCr plates under various loading conditions. In addition to measuring friction, the cartilage thickness was measured periodically throughout testing to quantify how much material was being removed. The study concluded that cartilage wear increased with contact stress, sliding distance and

sliding velocity. Interestingly, there was no clear relationship between the coefficient of friction and the linear wear of cartilage in longer testing protocols at low stress levels. The authors attributed this result to the multiphasic properties of cartilage.

The previous studies presented methods to assess *in vitro* wear without accounting for the effect of implant geometry, but a number of studies have examined the wear effects in specific hemiarthroplasty procedures. McCann et al. performed *in vitro* wear testing on the articular cartilage of the medial compartment of the knee using fresh bovine femoral condyles worn against bovine tibial surfaces and stainless steel plates[51]. The flexion facets of the condyles were maintained in order to preserve physiological geometry while being worn on a pendulum friction simulator. Contact pressures were measured using Fuji Film Pressure Sensitive Film®, and the loads were taken from British Standard knee gait profiles. The study concluded that friction may not be a good indication of wear under high loading conditions, but that contact stress is an important factor influencing wear.

Another study from the same group utilized a very similar apparatus, but with polyurethane (PU) as the potential hemiarthroplasty material, which was directly compared to stainless steel and a cartilage-on-cartilage articulation[46]. As previously discussed, it is suggested that an implant material with lower stiffness, closer to that of native cartilage, may reduce contact stresses and, by proxy, wear. The results showed significant reductions in contact stresses, which have been associated with reduced wear as the modulus of the PU plates decreased[51,52]. Similarly, another study by McCann et al. showed that conformity had a negative correlation with wear. Specifically, their study showed that wear increased with contact stress, and that low conformity caused high contact stress and vice versa, which emphasizes the importance of hemiarthroplasty implant sizing and shape selection[53].

Studies have also examined wear properties of different implant materials *in vivo*[54]. Cruess et al. and Cook et al. reported severe cartilage wear and fibrillation following the replacement of canine femoral patellar grooves with CoCr implants and severe canine acetabular wear was reported after the hemiarthroplasty preocedures[55,56].

Custers et al. reported that wear was also problematic for hemiarthroplasty in rabbits and goats[57,58]. These studies examined implants made of various materials, all of which resulted in poor clinical outcomes. Studies performed for smaller joints are limited, though an *in vivo* study did examine the effects of implanting finger hemiarthroplasty implants of various materials into the knees of rabbits, with similarly poor outcomes[59]. However, the use of compliant materials that more closely mimic the biphasic properties of cartilage, including hydrogels and Bionate®, has shown promising results for use in hemiarthroplasty procedures, though none of these materials are currently applied in clinical use[60-67].

1.5 Finite Element Modeling of Hemiarthroplasty Implants Against Cartilage

In vivo measurements of contact stresses and strains of the articular surfaces of synovial joints are often inaccurate and difficult to acquire[68]. However, since the 1970s, computational simulations capable of determining stresses, strains, contact areas, and forces have been employed for these purposes in biomechanics[69]. Advancements in imaging technology allow for accurate anatomical reconstruction of the bony anatomy of joints, and programs with high computational power have enabled accurate modeling bone and soft tissues. These methods are frequently used for stress analysis of intact joints, replaced joints, fracture fixation devices, and to examine the morphology and mechanical behavior of soft tissues[69].

Finite element modeling involves discretizing a complex, continuous component that is loaded into smaller elements, solving them, and linking them together so that a prediction of local stresses and strains of the elements can be determined. These "finite" elements can be assigned individual material properties that reflect the variation that occurs in the actual component.

These techniques have been used to examine articular contact mechanics in the elbow[70-72], the shoulder[73-75], the knee[76,77], and the hip[78,79]. Similarly, sophisticated models of soft tissues have been developed[80,81]. Complex models that simulate the biphasic properties of

cartilage that provide site-specific data are available, though they are computationally taxing and time consuming[82-86]. These models go as far as to provide stress distributions through the layers of cartilage by accounting for cartilage's varying mechanical properties, and have shown the time dependence of cartilage mechanics[87]. Some FEA models have even successfully simulated the removal of cartilage following wear in the intact knee joint[77], but wear following hemiarthroplasty has yet to be simulated in such a sophisticated manner.

A variety of these cartilage models have been used to investigate hemiarthroplasty contact mechanics. While most of these studies examine the effects of implant size and shape, the effect of hemiarthroplasty implant materials on cartilage stress has also been examined[88], though no significant differences among the investigated biomaterials were observed. Büchler et al. examined the effect of shape and size of shoulder hemiarthroplasty implants computationally in a FES that compared contact mechanics of an intact shoulder model to those of two commercially available humerus implants[89].

Finite element models have also been used to supplement *in vitro* hemiarthroplasty wear studies. McGann et al. analyzed shear stresses in a model that simulated cartilage undergoing sliding contact. The cartilage was modeled as a single phase elastic solid to help interpret the experimental data previously described[42]. Shear stresses acting along the midline of the articulation between a model that was loaded and reciprocated cartilage plugs against a steel plate were analyzed to assure that the contact pressure desired for the experimental tests was maintained for all testing configurations.

Neohookian hyperelastic cartilage models have been shown to be more accurate than single phase elastic models[90] and can be incorporated into two dimensional models that avoid the computational expense of three dimensional simulations without compromising accuracy[91]. As such, finite element analysis may be used to complement and enhance *in vitro* wear results by determining contact area, contact pressure, and stress concentration locations at the implant-cartilage interface of models that simulate hemiarthroplasty.

1.6 Rationale

Hemiarthroplasty procedures restore joint function, stability, and kinematics while minimizing patient morbidity and maximizing the preservation of native anatomy. However, these implants must optimize load transfer so as to minimize stresses and wear at the articular surface and improve clinical outcomes.

There is evidence that implant geometry can be optimized to reduce wear by increasing contact area and congruency with the adjacent articular cartilage[72,92]. The literature also suggests that more compliant hemiarthroplasty implant materials may reduce cartilage degeneration[36,46,56,93,94]. Though more compliant implant materials seem to produce less wear, the relationship between implant stiffness and damage to articular cartilage remains unclear. Specifically, whether there is a gradual increase in wear as implant stiffness increases, or if there is a threshold level at which contact mechanics shift detrimentally is not known.

The success of hemiarthroplasty and partial joint replacement systems depends on a more complete understanding of the effects of implant shape, size, and stiffness on cartilage wear, as well as on restoration of the joint's kinematics and stability. Further insight will be provided by comparing the results of *in vitro* wear tests with a complementary computational finite element analysis of the contact area and stresses at the implant-cartilage interface. These insights have implications on the design of various partial- and total hemiarthroplasty procedures.

In view of the foregoing, these studies were conducted to elucidate the relationships between hemiarthroplasty implant geometry and material and cartilage wear. Two *in vitro* studies utilized a pin-on-plate wear simulator that reciprocated hemiarthroplasty implant models against fresh frozen bovine articular cartilage. The topographical changes in the cartilage surfaces were used to determine volumetric wear, which was compared among groups. Additionally, contact areas and stresses at the implant-cartilage articulation were determined by a finite element simulation (FES).

1.7 Objectives and Hypotheses

1.7.1 Objectives

1. To develop an efficient and effective alternative to traditional methods of quantifying cartilage wear.
2. To quantify the effects of varying implant-cartilage contact area on cartilage damage.
3. To elucidate the effects of varying implant material on cartilage wear.
4. To relate *in vitro* wear results with cartilage stress levels using finite element analysis.

1.7.2 Hypotheses

1. A non-contact imaging protocol can be developed to reliably quantify cartilage wear and surface damage.

   Traditional methods for cartilage wear quantification are labour intensive and time consuming, and depend on a number of tenuous assumptions. We proposed that a non-contact imaging protocol would be an efficient alternative to traditional cartilage wear quantification methods.

2. Increasing articular contact area reduces wear on cartilage.

   Increasing articular contact area is predicted to reduce contact pressure and local stress concentrations, and, by proxy, cartilage erosion. Specifically, we propose that increasing the contact area at the implant-cartilage interface will decrease volumetric wear.

3. Reducing the stiffness of implant material reduces wear on adjacent articular cartilage.

   Though the relationship between implant stiffness and damage to articular cartilage remains unclear, it is hypothesized that more compliant implant materials will produce less wear. Therefore, this study seeks to elucidate

the relationship between hemiarthroplasty implant material stiffness and volumetric wear *in vitro*.

4. That increased articular contact area will decrease contact stresses acting on the cartilage.

    It is hypothesized that the finite element model will show an increase in average and peak stresses as:

    a) Implant-cartilage contact area decreases.
    b) Implant stiffness increases.

1.8 Thesis Overview

The forthcoming chapters detail they ways in which the aforestated objectives were met. Chapter 2 presents an *in vitro* examination of the effect of implant contact geometry on cartilage wear as well as a new method to assess cartilage wear. Chapter 3 uses the methods outlined in Chapter 2 to evaluate the effect of implant material stiffness on cartilage wear. In order to determine the stress levels at the implant-cartilage interface, a finite element study was conducted and is detailed in Chapter 4. Chapter 5 summarizes the conclusions of the presented studies as well as future research directions.

1.9 References

1. Lu X, Mow V. Biomechanics of articular cartilage and determination of material properties. *Medicine Science in Sports Exercise*. 2008;40(2):193.

2. Athanasiou K, Rosenwasser M, Buckwalter J, Malinin T, Mow V. Interspecies comparisons of in situ intrinsic mechanical properties of distal femoral cartilage. *Journal of Orthopaedic Research*. 1991;9(3):330-340.

3. Mansour JM. Biomechanics of cartilage. *Kinesiology: the mechanics and pathomechanics of human movement*. 2004;2:66-79.

4. Mansour JM. Biomechanics of cartilage. *Kinesiology: the mechanics and pathomechanics of human movement*. 2004;2:66-79.

5. Pawaskar SS, Ingham E, Fisher J, Jin Z. Fluid load support and contact mechanics of hemiarthroplasty in the natural hip joint. *Med Eng Phys*. 2011;33(1):96-105.

6. Radin E, Burr D, Caterson B, Fyhrie D, Brown T, Boyd R. Mechanical determinants of osteoarthrosis. . 1991;21(3):12-21.

7. Jin H, Lewis JL. Determination of poisson's ratio of articular cartilage by indentation using different-sized indenters. *J Biomech Eng*. 2004;126(2):138-145.

8. Johnson G, Dowson D, Wright V. The elastic behaviour of articular cartilage under a sinusoidally varying compressive stress. *Int J Mech Sci*. 1977;19(5):301-308.

9. Mansour JM, Mow VC. The permeability of articular cartilage under compressive strain and at high pressures. *J Bone Joint Surg Am*. 1976;58(4):509-516.

10. Lizhang J, Fisher J, Jin Z, Burton A, Williams S. The effect of contact stress on cartilage friction, deformation and wear. *Proc Inst Mech Eng Part H J Eng Med*. 2011;225(5):461-475.

11. An K, Morrey B. Biomechanics of the elbow. . In: Morrey B, ed. *The elbow and its disorders.* Third ed. WB Saunders Co.; 2001:43.

12. Gordon H, Larson S. Embryology and phylogeny. In: Morrey B, ed. *The elbow and its disorders.* Third ed. WB Saunders Co.; 2001:1-11.

13. An K, Morrey BF, Chao EY. The effect of partial removal of proximal ulna on elbow constraint. *Clin Orthop*. 1986;209:270-279.

14. Hotchkiss RN, Weiland AJ. Valgus stability of the elbow. *Journal of orthopaedic research*. 1987;5(3):372-377.

15. King GJ, Morrey BF, An K. Stabilizers of the elbow. *Journal of Shoulder and Elbow Surgery*. 1993;2(3):165-174.

16. Jobe CM. Gross anatomy of the shoulder. *The shoulder*. 1998;2.

17. Peat M. Functional anatomy of the shoulder complex. *Phys Ther*. 1986;66(12):1855-1865.

18. Culham E, Peat M. Functional anatomy of the shoulder complex. *Journal of Orthopaedic & Sports Physical Therapy*. 1993;18(1):342-350.

19. Howell SM, Galinat BJ, Renzi AJ, Marone PJ. Normal and abnormal mechanics of the glenohumeral joint in the horizontal plane. *J Bone Joint Surg Am*. 1988;70(2):227-232.

20. Poppen NK, Walker PS. Normal and abnormal motion of the shoulder. *J Bone Joint Surg Am*. 1976;58(2):195-201.

21. Gschwend N. Present state-of-the-art in elbow arthroplasty. *Acta Orthop Belg*. 2002;68(2):100-117.

22. Schneeberger AG, Meyer DC, Yian EH. Coonrad-morrey total elbow replacement for primary and revision surgery: A 2-to 7.5-year follow-up study. *Journal of Shoulder and Elbow Surgery*. 2007;16(3):S47-S54.

23. Wright TW, Wong AM, Jaffe R. Functional outcome comparison of semiconstrained and unconstrained total elbow arthroplasties. *Journal of Shoulder and Elbow Surgery*. 2000;9(6):524-531.

24. Burkhart KJ, Nijs S, Mattyasovszky SG, et al. Distal humerus hemiarthroplasty of the elbow for comminuted distal humeral fractures in the elderly patient. *The Journal of Trauma and Acute Care Surgery*. 2011;71(3):635-642.

25. Siguier T, Siguier M, Judet T, Charnley G, Brumpt B. Partial resurfacing arthroplasty of the femoral head in avascular necrosis: Methods, indications, and results. *Clin Orthop*. 2001;386:85-92.

26. Siguier M, Judet T, Siguier T, Charnley G, Brumpt B, Yugue I. Preliminary results of partial surface replacement of the femoral head in osteonecrosis. *J Arthroplasty*. 1999;14(1):45-51.

27. King GJ, Zarzour ZD, Rath DA, Dunning CE, Patterson SD, Johnson JA. Metallic radial head arthroplasty improves valgus stability of the elbow. *Clin Orthop*. 1999;368:114-125.

28. Grewal R, MacDermid JC, Faber KJ, Drosdowech DS, King GJ. Comminuted radial head fractures treated with a modular metallic radial head arthroplastyStudy of outcomes. *The Journal of Bone & Joint Surgery*. 2006;88(10):2192-2200.

29. Beingessner DM, Dunning CE, Gordon KD, Johnson JA, King GJ. The effect of radial head excision and arthroplasty on elbow kinematics and stability. *The Journal of Bone & Joint Surgery*. 2004;86(8):1730-1739.

30. Sabo M, Shannon H, De Luce S, et al. Elbow kinematics after radiocapitellar arthroplasty. *J Hand Surg*. 2012;37(5):1024-1032.

31. Maghen Y, Leo AJ, Hsu JW, Hausman MR. Is a silastic radial head still a reasonable option? *Clinical Orthopaedics and Related Research®*. 2011;469(4):1061-1070.

32. Liew VS, Cooper IC, Ferreira LM, Johnson JA, King GJ. The effect of metallic radial head arthroplasty on radiocapitellar joint contact area. *Clin Biomech*. 2003;18(2):115-118.

33. McGibbon C, Krebs D, Trahan C, Trippel S, Mann R. Cartilage degeneration in relation to repetitive pressure: Case study of a unilateral hip hemiarthroplasty patient. *J Arthroplasty*. 1999;14(1):52-58.

34. Moon KH, Kang JS, Lee TJ, Lee SH, Choi SW, Won MH. Degeneration of acetabular articular cartilage to bipolar hemiarthroplasty. *Yonsei Med J*. 2008;49(5):719-724. doi: 10.3349/ymj.2008.49.5.719; 10.3349/ymj.2008.49.5.719.

35. Patwari P, Gaschen V, James I, et al. Ultrastructural quantification of cell death after injurious compression of bovine calf articular cartilage. *Osteoarthritis and cartilage*. 2004;12(3):245-252.

36. Aigner T, McKenna L. Molecular pathology and pathobiology of osteoarthritic cartilage. *Cellular and Molecular Life Sciences CMLS*. 2002;59(1):5-18.

37. Patwari P, Cook MN, DiMicco MA, et al. Proteoglycan degradation after injurious compression of bovine and human articular cartilage in vitro: Interaction with exogenous cytokines. *Arthritis & Rheumatism*. 2003;48(5):1292-1301.

38. Giannicola G, Sacchetti FM, Antonietti G, Piccioli A, Postacchini R, Cinotti G. Radial head, radiocapitellar and total elbow arthroplasties: A review of recent literature. *Injury*. 2013.

39. Moungondo F, El Kazzi W, van Riet R, Feipel V, Rooze M, Schuind F. Radiocapitellar joint contacts after bipolar radial head arthroplasty. *Journal of shoulder and elbow surgery*. 2010;19(2):230-235.

40. Van Riet RP, Van Glabbeek F, Verborgt O, Gielen J. Capitellar erosion caused by a metal radial head prosthesisA case report. *The Journal of Bone & Joint Surgery Case Connector*. 2004;86(5):1061-1064.

41. Calfee R, Madom I, Weiss AC. Radial head arthroplasty. *J Hand Surg*. 2006;31(2):314-321.

42. McGann ME, Vahdati A, Wagner DR. Methods to assess in vitro wear of articular cartilage. *Proc Inst Mech Eng Part H J Eng Med*. 2012;226(8):612-622.

43. Chan S, Neu C, Komvopoulos K, Reddi A, Di Cesare P. Friction and wear of hemiarthroplasty biomaterials in reciprocating sliding contact with articular cartilage. *Journal of tribology*. 2011;133(4).

44. Forster H, Fisher J. The influence of loading time and lubricant on the friction of articular cartilage. *Proc Inst Mech Eng Part H J Eng Med*. 1996;210(2):109-119.

45. Lipshitz H, Etheredge R,3rd, Glimcher MJ. In vitro wear of articular cartilage. *J Bone Joint Surg Am*. 1975;57(4):527-534.

46. Luo Y, McCann L, Ingham E, Jin Z, Ge S, Fisher J. Polyurethane as a potential knee hemiarthroplasty biomaterial: An in-vitro simulation of its tribological performance. *Proc Inst Mech Eng Part H J Eng Med*. 2010;224(3):415-425.

47. Northwood E, Fisher J. A multi-directional in vitro investigation into friction, damage and wear of innovative chondroplasty materials against articular cartilage. *Clin Biomech*. 2007;22(7):834-842.

48. Radin EL, Swann DA, Paul IL, Mcgrath PJ. Factors influencing articular cartilage wear in vitro. *Arthritis & Rheumatism*. 1982;25(8):974-980.

49. Weightman B. In vitro fatigue testing of articular cartilage. *Ann Rheum Dis*. 1975;34(Suppl 2):108-110.

50. Emery I, Meachim G. Surface morphology and topography of patello-femoral cartilage fibrillation in liverpool necropsies. *J Anat*. 1973;116(Pt 1):103.

51. McCann L, Udofia I, Graindorge S, Ingham E, Jin Z, Fisher J. Tribological testing of articular cartilage of the medial compartment of the knee using a friction simulator. *Tribol Int*. 2008;41(11):1126-1133.

52. Johnson JA, Beingessner DM, Gordon KD, Dunning CE, Stacpoole RA, King GJ. Kinematics and stability of the fractured and implant-reconstructed radial head. *Journal of shoulder and elbow surgery*. 2005;14(1):S195-S201.

53. McCann L, Ingham E, Jin Z, Fisher J. An investigation of the effect of conformity of knee hemiarthroplasty designs on contact stress, friction and degeneration of articular cartilage: A tribological study. *J Biomech*. 2009;42(9):1326-1331.

54. Laberge M, Dennis Bobyn J, Drouin G, Rivard CH. Evaluation of metallic personalized hemiarthroplasty: A canine patellofemoral model. *J Biomed Mater Res*. 1992;26(2):239-254.

55. Cruess RL, Kwok DC, Duc PN, Lecavalier M, Dang G. The response of articular cartilage to weight-bearing against metal. *J Bone Joint Surg Br*. 1984;4:592-597.

56. Cook S, Thomas KA, Kester MA. Wear characteristics of the canine acetabulum against different femoral prostheses. *Journal of Bone & Joint Surgery, British Volume*. 1989;71(2):189-197.

57. Custers R, Dhert W, van Rijen M, Verbout A, Creemers L, Saris D. Articular damage caused by metal plugs in a rabbit model for treatment of localized cartilage defects. *Osteoarthritis and Cartilage*. 2007;15(8):937-945.

58. Custers R, Dhert W, Saris D, et al. Cartilage degeneration in the goat knee caused by treating localized cartilage defects with metal implants. *Osteoarthritis and Cartilage*. 2010;18(3):377-388.

59. Jung M, Wieloch P, Lorenz H, et al. Comparison of cobalt chromium, ceramic and pyrocarbon hemiprostheses in a rabbit model: Ceramic leads to more cartilage damage than cobalt chromium. *Journal of Biomedical Materials Research Part B: Applied Biomaterials*. 2008;85(2):427-434.

60. Oka M, Ushio K, Kumar P, et al. Development of artificial articular cartilage. *Proc Inst Mech Eng H*. 2000;214(1):59-68.

61. Murakami T, Higaki H, Sawae Y, Ohtsuki N, Moriyama S, Nakanishi Y. Adaptive multimode lubrication in natural synovial joints and artificial joints. *Proc Inst Mech Eng H*. 1998;212(1):23-35.

62. Nakashima K, Sawae Y, Tsukamoto N, Miura H, Iwamoto Y, Murakami T. Wear behaviour of an artificial cartilage material for hemiarthroplasty. . 2010:1169-1172.

63. Suciu AN, Iwatsubo T, Matsuda M, Nishino T. A study upon durability of the artificial knee joint with PVA hydrogel cartilage. *JSME International Journal Series C Mechanical Systems, Machine Elements and Manufacturing*. 2004;47(1):199-208.

64. Gong JP, Osada Y. Soft and wet materials: From hydrogels to biotissues. In: *High solid dispersions.* Springer; 2010:203-246.

65. Bichara DA, Bodugoz-Sentruk H, Ling D, Malchau E, Bragdon CR, Muratoglu OK. Osteochondral defect repair using a polyvinyl alcohol-polyacrylic acid (PVA-PAAc) hydrogel. *Biomedical Materials*. 2014;9(4):045012.

66. Bichara DA, Zhao X, Bodugoz-Senturk H, et al. Porous poly (vinyl alcohol)-hydrogel matrix-engineered biosynthetic cartilage. *Tissue Engineering Part A*. 2010;17(3-4):301-309.

67. Bodugoz-Senturk H, Macias CE, Kung JH, Muratoglu OK. Poly (vinyl alcohol)–acrylamide hydrogels as load-bearing cartilage substitute. *Biomaterials*. 2009;30(4):589-596.

68. Winby CR, Lloyd DG, Besier TF, Kirk TB. Muscle and external load contribution to knee joint contact loads during normal gait. *J Biomech*. 2009;42(14):2294-2300.

69. Huiskes R, Chao E. A survey of finite element analysis in orthopedic biomechanics: The first decade. *J Biomech*. 1983;16(6):385-409.

70. Willing RT, Lalone EA, Shannon H, Johnson JA, King GJ. Validation of a finite element model of the human elbow for determining cartilage contact mechanics. *J Biomech*. 2013;46(10):1767-1771.

71. Pistoia W, Van Rietbergen B, Lochmüller E, Lill C, Eckstein F, Rüegsegger P. Estimation of distal radius failure load with micro-finite element analysis models based on three-dimensional peripheral quantitative computed tomography images. *Bone*. 2002;30(6):842-848.

72. Langohr G, Willing R, Medley J, King G, Johnson J. Finite element contact analysis of axisymmetric and non-axisymmetric radial head hemiarthroplasty. *Orthopaedic Research Society Annual Meeting*. 2013.

73. Büchler P, Ramaniraka N, Rakotomanana L, Iannotti J, Farron A. A finite element model of the shoulder: Application to the comparison of normal and osteoarthritic joints. *Clin Biomech*. 2002;17(9):630-639.

74. Friedman RJ, LaBerge M, Dooley RL, O'Hara AL. Finite element modeling of the glenoid component: Effect of design parameters on stress distribution. *Journal of Shoulder and Elbow Surgery*. 1992;1(5):261-270.

75. Petraglia CA, Ramirez MA, Tsai MA, Parks BG, Murthi AM. Glenohumeral pressure with surface replacement arthroplasty versus hemiarthroplasty. *Orthopedics (Online)*. 2014;37(10):e892.

76. Bendjaballah MZ, Shirazi-Adl A, Zukor D. Finite element analysis of human knee joint in varus-valgus. *Clin Biomech*. 1997;12(3):139-148.

77. Li L, Patil S, Steklov N, et al. Computational wear simulation of patellofemoral articular cartilage during< i> in vitro testing. *J Biomech*. 2011;44(8):1507-1513.

78. Anderson AE, Ellis BJ, Maas SA, Weiss JA. Effects of idealized joint geometry on finite element predictions of cartilage contact stresses in the hip. *J Biomech*. 2010;43(7):1351-1357.

79. Anderson AE, Ellis BJ, Maas SA, Peters CL, Weiss JA. Validation of finite element predictions of cartilage contact pressure in the human hip joint. *J Biomech Eng*. 2008;130(5):051008.

80. Zhang M, Zheng Y, Mak AF. Estimating the effective young's modulus of soft tissues from indentation tests—nonlinear finite element analysis of effects of friction and large deformation. *Med Eng Phys*. 1997;19(6):512-517.

81. Wakabayashi I, Itoi E, Sano H, et al. Mechanical environment of the supraspinatus tendon: A two-dimensional finite element model analysis. *Journal of shoulder and elbow surgery*. 2003;12(6):612-617.

82. Goldsmith A, Hayes A, Clift SE. Application of finite elements to the stress analysis of articular cartilage. *Med Eng Phys*. 1996;18(2):89-98.

83. Mow VC, Ratcliffe A, Poole AR. Cartilage and diarthrodial joints as paradigms for hierarchical materials and structures. *Biomaterials*. 1992;13(2):67-97.

84. Clift SE. Finite-element analysis in cartilage biomechanics. *J Biomed Eng*. 1992;14(3):217-221.

85. Hosoda N, Sakai N, Sawae Y, Murakami T. Finite element analysis of articular cartilage model considering the configuration and biphasic property of the tissue. . 2009:1883-1887.

86. Wu J, Herzog W, Epstein M. Evaluation of the finite element software ABAQUS for biomechanical modelling of biphasic tissues. *J Biomech*. 1997;31(2):165-169.

87. Manda K, Eriksson A. Time-dependent behavior of cartilage surrounding a metal implant for full-thickness cartilage defects of various sizes: A finite element study. *Biomechanics and Modeling in Mechanobiology*. 2012;11(5):731-742.

88. Reeves J, Razfar N, Langohr G, Athwal G, King G, Johnson J. The effect of material selection and implant positioning on cartilage stresses following partial joint resurfacing: A finite element study. *Orthopaedic Research Society Annual Meeting*. 2015(Montreal, Quebec).

89. Büchler P, Farron A. Benefits of an anatomical reconstruction of the humeral head during shoulder arthroplasty: A finite element analysis. *Clin Biomech*. 2004;19(1):16-23.

90. Büchler P, Ramaniraka N, Rakotomanana L, Iannotti J, Farron A. A finite element model of the shoulder: Application to the comparison of normal and osteoarthritic joints. *Clin Biomech*. 2002;17(9):630-639.

91. Cilingir A, Ucar V, Kazan R. Three-dimensional anatomic finite element modelling of hemi-arthroplasty of human hip joint. *Trends Biomater Artif Organs*. 2007;21(1):63-72.

92. Lalone EA, McDonald CP, Ferreira LM, Peters TM, King GW, Johnson JA. Development of an image-based technique to examine joint congruency at the elbow. *Comput Methods Biomech Biomed Engin*. 2013;16(3):280-290.

93. Foy JR, Williams PF,3rd, Powell GL, Ishihara K, Nakabayashi N, LaBerge M. Effect of phospholipidic boundary lubrication in rigid and compliant hemiarthroplasty models. *Proc Inst Mech Eng H*. 1999;213(1):5-18.

94. Dalldorf PG, Banas MP, Hicks DG, Pellegrini V. Rate of degeneration of human acetabular cartilage after hemiarthroplasty. *The Journal of Bone & Joint Surgery*. 1995;77(6):877-882.

Chapter 2

The Effect of Hemiarthroplasty Implant Geometry on Early *In Vitro* Cartilage Wear

OVERVIEW: *This chapter presents a study that examines the effect of implant geometry on early in vitro cartilage wear. In order to isolate the effect of contact area, pin models with varying radii of curvature were reciprocated against cartilage explants using a pin-on-plate wear simulator and the volumetric wear was compared. A novel methodology to quantify cartilage wear is introduced.*

This work was presented at the 2015 Annual Meeting of the Canadian Orthopaedic Research Society and at the 2015 Annual Meeting of the Orthopaedic Research Society.

2.1 Introduction

As stated in Chapter 1, complication and failure rates of total arthroplasty in the upper limbs are higher than in the lower limbs because of the invasive surgical techniques required for their implantation[1-3]. In cases where only one articulating surface of a synovial joint is damaged, partial replacements (hemiarthroplasties) have proven to be viable alternatives to total joint replacement. These procedures, where only one of the articulating surfaces of a joint is replaced, restore joint function, stability, and kinematics while maximizing bone and cartilage preservation[4]. However, it is important these implants optimize load transfer so as to minimize peak stresses at the articular surface to prevent wear in the adjacent articular cartilage that may necessitate surgical revision.

For example, the clinical success of a prevalent hemiarthroplasty procedure, radial head replacement, is compromised by poor contact mechanics between the implant and the adjacent articular cartilage[5-7]. While these replacements restore joint kinematics, their stiffness and lack of congruity with the native counter-surface cause a decrease in contact

area. For example, a drop in contact area of two-thirds has been reported in metallic unipolar radial head implants and this produces greater contact pressures[8] at the implant-cartilage interface. Unfortunately, it has been reported that areas subject to higher contact pressures are associated with increased cartilage degeneration[9]. Furthermore, increases in contact stress have been shown to promote the secretion of degenerative enzymes, which have a deteriorative effect on the stiffness and elasticity of articular cartilage[10]. Degenerative changes to the capitellar surface, or wear, commonly follow elbow hemiarthroplasty[11-13], so the implantation of these devices is generally limited to older, relatively inactive patients when possible[6,14].

These factors contribute to suboptimal clinical outcomes for hemiarthroplasty procedures despite their reduced cost, simplified surgical approach, and preservation of native anatomy. The clinical need for hemiarthroplasty procedures is clear, but the understanding and improvement of implant-cartilage contact mechanics is necessary to improve their performance, increase their longevity, and broaden their clinical applicability.

There is evidence that implant geometry may be optimized to reduce wear by increasing contact area and congruency with the adjacent articular cartilage. Tribological simulations conducted using pin-on-disk wear simulators have established testing conditions[15] and evaluated potential hemiarthroplasty materials on cartilage[16,17]. Furthermore, studies have utilized more sophisticated devices to maintain joint geometry[18,19] but an assessment of the direct effect of contact geometry on the wear of cartilage was not performed.

The purpose of the present study was to investigate the effect of hemiarthroplasty implant shape on the wear of cartilage specimens in linear reciprocal sliding using a novel non-contact imaging protocol. It was hypothesized that increasing articular contact area would reduce contact pressure and local stress concentrations, and, by proxy, cartilage erosion. Specifically, we proposed that increasing the contact area at the implant-cartilage interface would decrease volumetric wear as well as the depth of the resultant wear track.

2.2 Materials and Methods

Stainless steel pins of varying radii of curvature (ROC) were selected as hemiarthroplasty implant models. Their ROC, depicted in Figure 2-1, ranged from hemispherical (ROC=4.70 mm) to nearly planar (ROC=11.7 mm). A completely planar pin was also examined, but the results were excluded due to disproportionate damage caused by the tip's edges. The pins were machined and polished to the desired geometry at University Machine Services at the University of Western Ontario, then soaked in a diluted isopropyl alcohol solution to remove any debris and embedded particles from the surfaces.

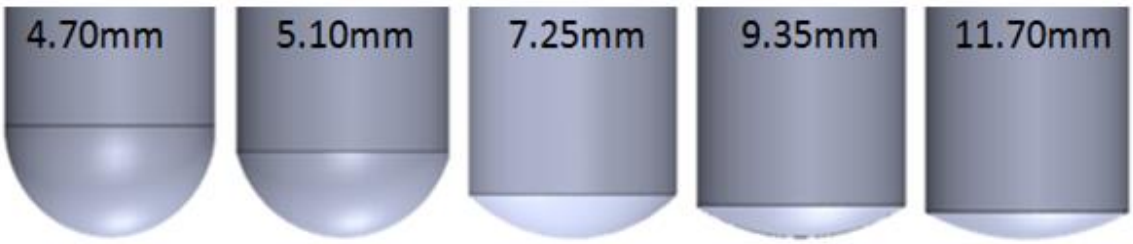

Figure 2-1 *Implant models with radii of curvature. E=200 GPa, v=0.28.*

The pins were custom made from AISI 304 stainless steel with a Young's modulus of 200 GPa, polished to a surface roughness R_a of 1.9 μm and examined by scanning electron microscopy (Appendix B).

2.2.1 Tissue Acquisition and Preparation

Cylindrical plugs of articular cartilage and underlying subchondral bone were harvested from the proximal faces of bovine radii and ulnae obtained from a local abattoir (Ralph Bos Meats Ltd, Strathroy, ON) and frozen at -20ºC within 12 hours of death. Indentation testing has shown that freezing and thawing under these conditions does not alter the mechanical properties of cartilage[20-23]. Moreover, no significant differences were observed in a direct comparison of volumetric wear among fresh and fresh frozen cartilage specimens we conducted to establish a specimen preparation protocol (detailed in Appendix C). A 25 mm diameter diamond-tip hole saw was used to extract a 5 mm deep

cylindrical explant of cartilage and underlying subchondral bone, one each from the ulnar and radial sides of the joint. For each implant model, half of the explants were taken from the superior faces of radius, and the other from the ulna. The provenance of the explant was recorded and randomized to examine its effect on wear.

The explants were potted into custom jigs using Instant Tray Mix (Lang Dental Mfg Co., Inc., Illinois) so that the flexion-extension axis of the joint would be aligned with the direction of wear. Once fixed into the jig, the cartilage surface was scanned using a non-contact 3D scanner (NextEngine, Santa Monica, California) to generate a mesh representative of the unworn cartilage surface. Before testing, the explants were submerged in phosphate buffered saline (PBS) to prevent dehydration.

2.2.2 Tribological Simulation

For the duration of testing, the explants were submerged in a lubricant consisting of HyClone™ Alpha Calf Fraction Serum Supplement (ACS; GE Healthcare Life Sciences, Utah, USA) with an original protein concentration of 38 g/L[24], diluted with PBS to a protein concentration of 17g/L in accordance to ISO standards[25].The lubricant also contained a 1% concentration of Antibiotic-Antimycotic (Invitrogen, Mississauga, ON). ACS was used because of the similarity of its protein constituent fractions to those of synovial fluid[26]. The experiments were conducted at 22 ºC.

Specimens were worn using a six station pin-on-plate wear simulator in linear reciprocal sliding (Figure 2-2). Loads of 27.5 N were applied to the pins (n=8 for each tip geometry), which slid against the cartilage explants at a frequency of 1.2 Hz and a 10 mm stroke length for 140 minutes, at which point damage to the articular cartilage was visible on all cartilage explants. This corresponded to 10000 cycles on the simulator. The duration of testing was established by a study which examined the time dependence of cartilage wear as described in Appendix D. A linear increase of volumetric wear was observed as the number of cycles on the wear simulator increased, and at 10000 cycles, while surface damage was visible on all specimens, none had worn entirely through the cartilage to the subchondral bone. Accordingly, this duration was deemed adequate for the tribiological simulation.

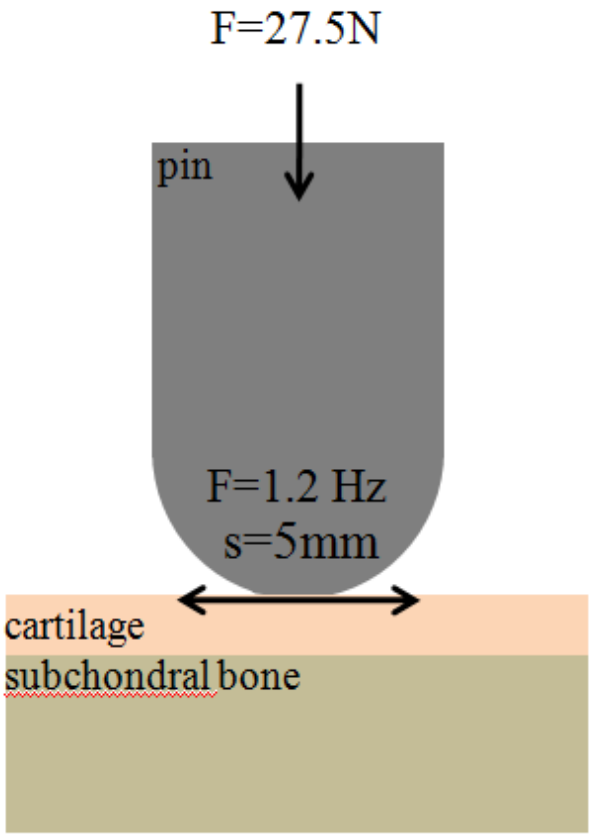

Figure 2-2 *Configuration of the pin on plate loading configuration: a constant 27.5 N load was applied to the face of the cartilage via a hemiarthroplasty implant model, the pin. This pin reciprocated against the cartilage at a rate 1.2 Hz with a 5 mm stroke length.*

The 27.5 N load that was selected produced stress levels in the cartilage within the clinically relevant range for various hemiarthroplasty procedures for all of the implant models that were investigated. The details of the load selection and a comparison of resultant stress levels and contact area among implant models and clinically implemented hemiarthroplasties are outlined in Appendix E and F respectively.

One additional explant was loaded statically for the duration of testing for each of the implant models to examine the effects of creep, or cartilage deformation under constant load. The depth of the indentation was measured. Once the load was removed, the explant was re-submerged in PBS, and the time until the cartilage surface regained its shape was measured. After the wear tests, the worn explants were submerged in PBS for that

duration of time so that topographic changes in the cartilage surface would represent volumetric wear as opposed to deformation. The details of the creep tests are included in Appendix G.

2.2.3 Wear Quantification

Wear was quantified by the volume of material removed and the average depth of the wear tracks that were produced during testing. These values were measured by comparing three dimensional scans taken of the cartilage explant surfaces before and after testing.

Immediately after testing, the specimens were rinsed with PBS to remove any wear debris or loose-hanging cartilage. After being submerged in PBS to remove the effects of creep, the explants, still potted, were re-scanned using the 3D scanner under identical settings. The macro range precision setting for the scanner was used, which produced point clouds with an accuracy of 0.127 mm, containing 26 points/mm^2. The pointclouds were exported as triangular element meshes with 0.191 mm edge lengths.

The full-colour scans were exported as meshes in .ply extension format.

Four landmarks on each cartilage explant surface were used to align the pre- and post-wear scans in MeshLab. A custom inter-surface distance algorithm written in VTK calculated the distance between the vertices of the triangular meshes (see Appendix H). In the unworn regions, the vertices of the aligned meshes have the same coordinates, so the distance between them is zero. In the worn regions, the distance between the corresponding points on the registered surfaces represents the depth of the damage at a given point. The normal distance from the centroid of each triangle on the unworn surface to the closest point on the worn surface was multiplied by the area of each triangular mesh element, and then summed over the entire surface to compute the total wear volume. The average wear depth was calculated by dividing the volumetric wear by the known contact area between the implant model and the cartilage surface.

Eight cartilage plugs were tested for each implant model. The data were analyzed using one way ANOVA with Kruskal-Wallis multiple comparisons to determine if any significantly different results could be observed among groups.

2.3 Results

The results are displayed graphically as the mean (n=8) ± standard deviation. All contact geometries investigated produced visible evidence of cartilage wear. Figure 2-3 shows the pre- and post- wear 3D scans along with a colour-contour map that visualizes the distance between the registered surfaces for a characteristic cartilage sample worn with the 4.70mm ROC pin.

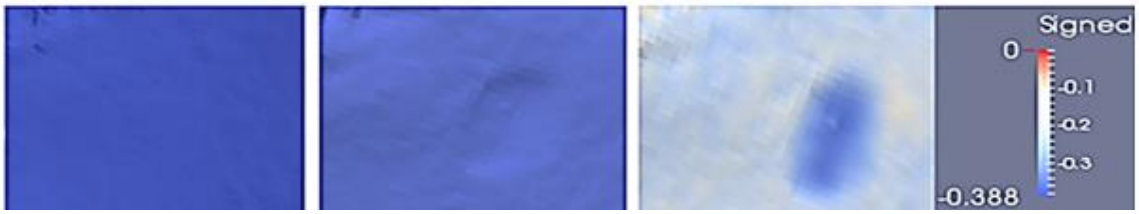

a b c

Figure 2-3 *Profiles of a characteristic cartilage surface: a) Scan of unworn cartilage surface b) Scan of worn cartilage surface c) Colour-contour map showing distance between worn and unworn surfaces.*

Figure 2-4 shows the volumetric wear (mean with standard deviation bars) for each of the implant model geometries. As predicted, the implant model with the greatest radius of curvature (ROC=11.7 mm) wore away significantly less cartilage than all implant models except the 9.35 mm radius of curvature model ($p<0.05$).

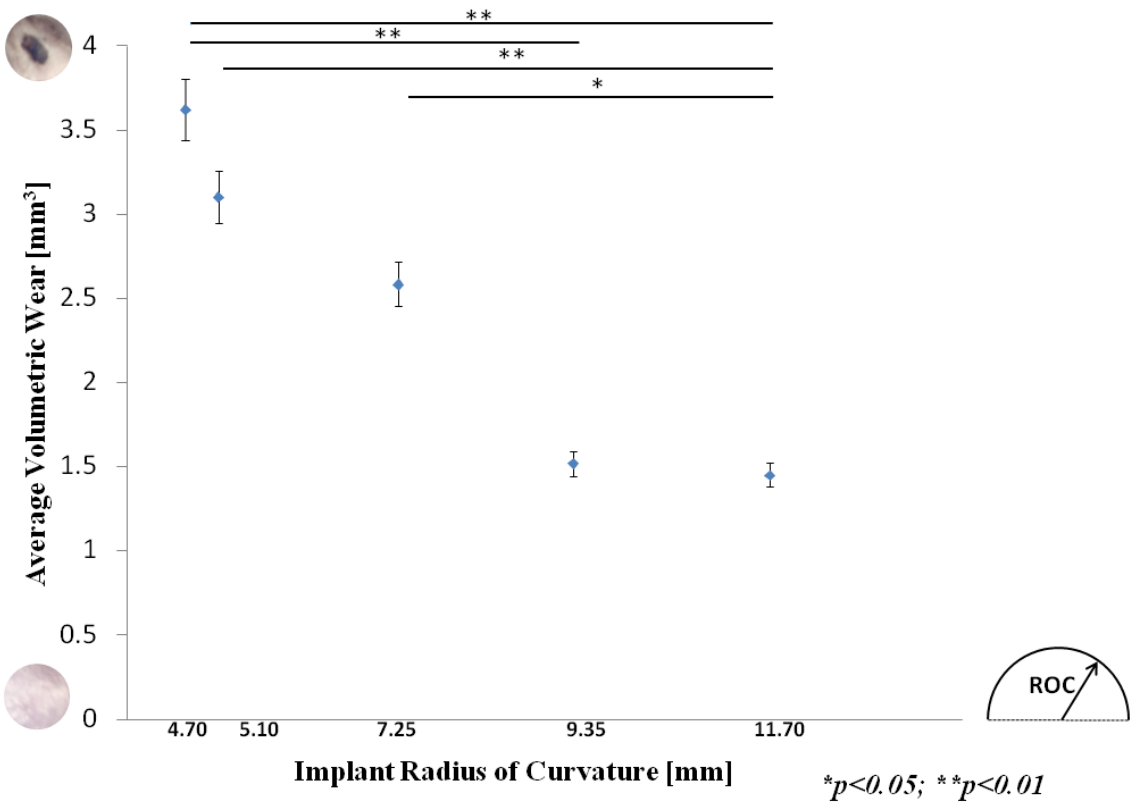

Figure 2-4 *Average volumetric wear caused by each implant model shown as a function of implant radius of curvature (ROC). The implant models with the greatest ROC produced significantly less cartilage wear than the implant models with the smaller ROC which suggests that cartilage damage is negatively related to implant-cartilage contact area (*p<0.05; **p<0.01).*

The flattest models (ROC=11.70 mm and ROC=9.35 mm) also produced significantly shallower ($p<0.05$) wear tracks in the cartilage than the other three implant models, as shown by Figure 2-5, in which the average wear depth for each geometry is presented. No statistically significant differences were detected in the wear between specimens harvested from the ulnar and radial sides of the joint.

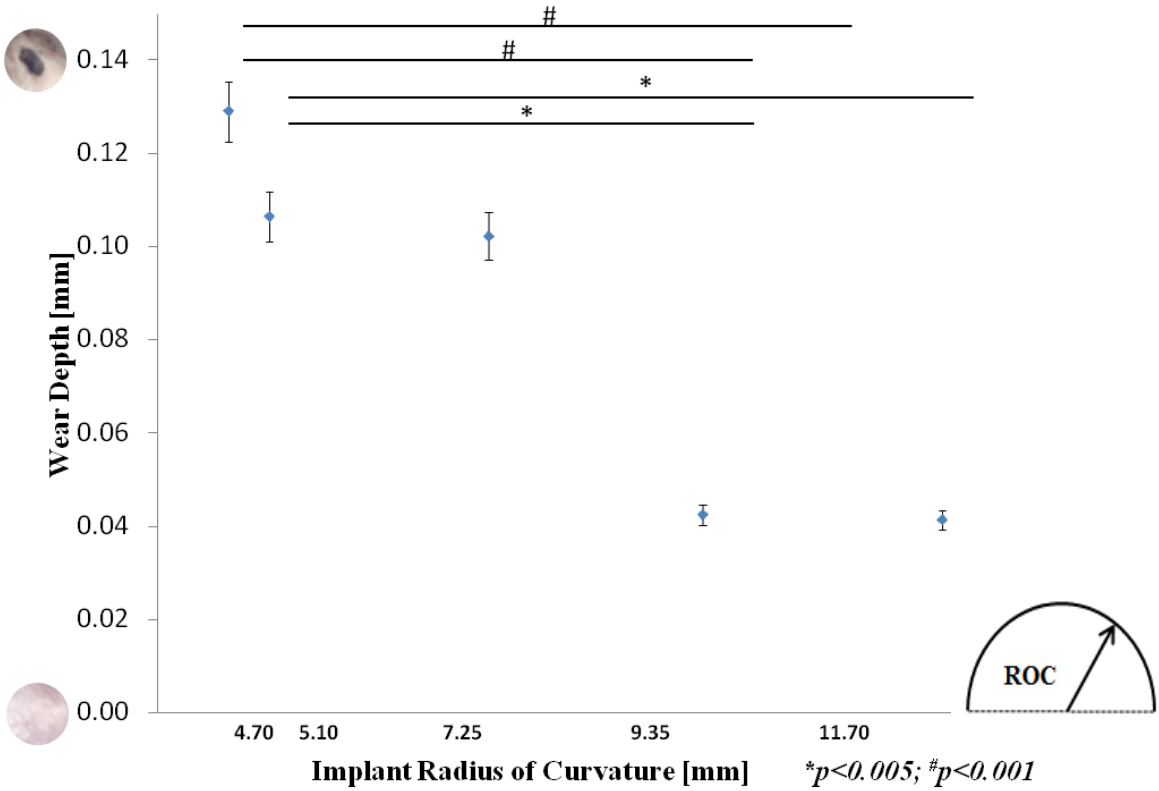

Figure 2-5 *Average wear depth caused by each implant mode shown as a function of implant radius of curvature (ROC). A highly significant increase in depth of the wear tracks produced was observed between the two flattest tipped pins ROC=9.35 mm and ROC=11.7 mm and the two roundest pins (ROC=4.70 mm and ROC=5.10 mm) which indicates a reduction in cartilage damage occurs as contact area increases (*p<0.005; #p<0.001).*

The worn specimens were also stained using India ink and photographed to provide a qualitative assessment of cartilage damage. India ink has been shown to adhere to fibrillated cartilage[15,27], which is a clear indicator of wear[16]. The specimens worn with the rounder tips (ROC=4.70 mm and ROC=5.10 mm) had more acute damage, as indicated by denser pigmentation, shown in Figure 2-6, which displays representative stained surfaces of samples from each sample group in order of increasing implant model radius of curvature.

Figure 2-6 *India ink stains of cartilage specimens in order of increasing radius of curvature in mm. Denser pigmentation indicates more severe wear, which decreased as radius of curvature increased.*

2.4 Discussion

The purpose of this study was to elucidate the relationship between the contact area of hemiarthroplasty implant models and the wear they induced on articular cartilage. As expected, an increase in volumetric wear was observed as the implant model-cartilage contact area decreased for the three roundest lower ROC pins. This can likely be attributed to the reduction of contact stress magnitudes that result from the increase in contact area. The pin with the smallest radius of curvature, which was hemispherical with a radius of 4.70 mm, removed significantly more material than the nearly planar 11.7 mm radius of curvature pin and the 9.25 mm radius of curvature pin ($p<0.01$). Similarly, the 5.10 mm tip pin wore away significantly more cartilage than the 11.7 mm tip pin ($p<0.01$). Finally, the 7.25 mm tip pin wore away significantly more cartilage than the 11.7 mm tip pin ($p<0.05$).

However, this trend does not appear to be linear because the last two higher ROC pins produced nearly identical wear. It appears that there are different wear regimes at the higher and lower ranges of radii because between ROC=4.70 mm and ROC= 7.25 mm, the decrease in wear is dramatic whereas between ROC=9.35 mm and ROC=11.7 mm, there is a negligible decrease in wear. This suggests that between the 7.25 mm and 9.35 mm radii implants, there is a shift in contact mechanics that reduces the wear sensitivity of cartilage to ROC. Figure 2-7 shows regions where separate wear trends occur for the volumetric wear results previously presented in Figure 2-4. This emphasizes the importance of maximizing articular contact area between cartilage and hemiarthroplasty implant especially if this sort of detrimental shift in contact mechanics observed in the

pin-on-plate configuration occurs *in vivo*, as severely accelerated wear will occur in patients. Interestingly, however, the results also suggest that once the alleged threshold zone is passed, the ROC does not have that much of an effect on wear, which could enable more versatility in the design of HA implant systems. Similar trends occurred for wear track depth.

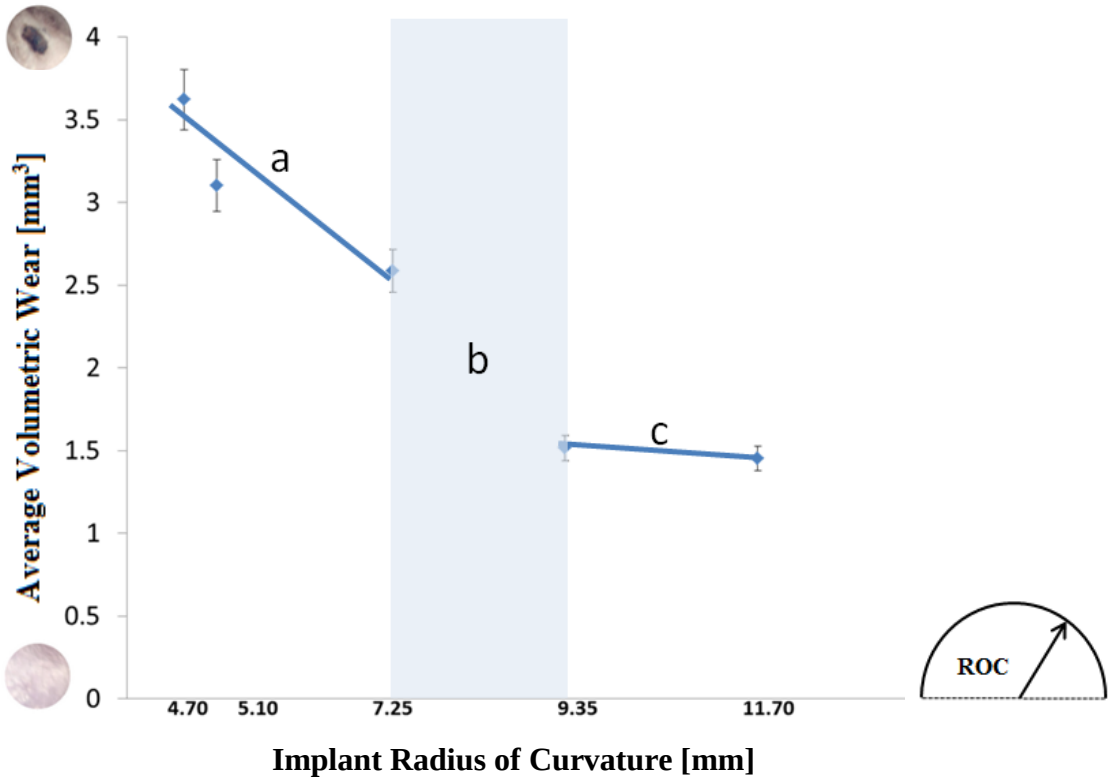

Figure 2-7 *Wear behaviour at different ranges of radius of curvature (ROC). a) Region of apparent high wear sensitivity to radius of curvature. b) Possible threshold region where shift in contact mechanics occurs. c) Region where wear apparently loses sensitivity to radius of curvature.*

While the differences observed for volumetric wear were statistically significant, greater differences were observed among samples for wear depth. Average wear depth was calculated by taking the net volumetric wear and normalizing it by the area of the wear track. This was used as an additional metric for cartilage damage since the staining of the cartilage surfaces showed fibrillation in the specimens that were worn using the rounder tipped hemiarthroplasty implant models (ROC=4.70 mm, ROC=5.10 mm, and ROC=7.25 mm) that appeared disproportionate to the net wear. While the more planar

implant models removed measurable amounts of cartilage, the damage to the cartilage surface did not appear to be as severe, as it was spread over a greater area and appeared to be uniform, as highlighted by the India ink staining protocol.

The lowest ROC pins, ROC=4.70 mm, ROC=5.10 mm, and ROC=7.25 mm produced significantly deeper wear tracks than the 9.35 mm and 11.70 mm ROC pins ($p<0.001$, $p<0.005$, and $p<0.05$, respectively), all with much higher percentage changes than were observed among groups for volumetric wear.

These results agree with similar *in vitro* studies that examined the role of contact stress on tribological cartilage degeneration. In an investigation of the effects of contact stress on cartilage wear and friction, Lizhang et al. found that in early cartilage wear, under the same contact stresses, smaller diameter cartilage pins worn against a cobalt chromium alloy (CoCr) plate produced significantly higher coefficients of friction than larger cartilage pins under lower loads[28]. The study also concluded that wear increased significantly with contact stress. Along the same lines, McCann et al. reported that increasing contact stress at the cartilage-implant interface increased friction, which may contribute to the degradation of collagen and proteoglycans as well as disrupt fluid film support[17]. Bonnevie et al. reported that at relatively low sliding speeds (under 5 mm/s), the friction coefficient between a sphere-tipped stainless steel indenter and bovine cartilage is proportional to contact area (viz. varying indented ROC), but that friction was independent of contact area at faster reciprocation rates[29]. The present study's pins reciprocated at a speed of 12 mm/s, which would be classified as 'high' speed by the Bonnevie et al. study, which would make friction independent of pin contact area. It can be inferred from the findings of these two studies that macro-scale cartilage wear would be inversely proportional to contact area, which supports the findings of the present study.

Sathasivam et al. conducted an *in vitro* examination of the effect of varying contact area in total knee replacement under the same hypothesis as was examined in this study; namely, that increased contact area reduces wear rates[30]. Flat-faced UHMWPE pins of varying diameter were worn against flat CoCr trays under a constant load in rotation and reciprocal sliding. The study concluded that increased contact area produced lower wear

rates, and, interestingly, in the larger diameter pins tested, milder wear processes. Though this study did not involve articular cartilage, its findings agree with the more severe fibrillation observed in the cartilage worn by the hemiarthroplasty implant models with the smaller radii of curvature.

Wear in orthopedics is typically quantified by the mass difference in samples taken before and after testing but the high water content of cartilage makes direct mass comparison for cartilage difficult and inaccurate. The "gold standard" for cartilage wear assessment involves estimating the mass of cartilage removed based on the protein content of the lubricating bath after testing, then expressing it as a function of cartilage's original surface area or volume. The mass of cartilage worn off of the specimen can be inferred from the hydroxyproline content of the lubricating fluid based on the assumption that it accounts for about 7.8% of the dry weight of bovine cartilage[15].

As previously mentioned, India ink has been used in semi-quantitative cartilage wear assessment. McGann et al. reported a high correlation between wear rates measured using the "gold standard" mass analysis and an India ink staining protocol. After staining, McGann et al. assessed wear by assigning a threshold to each image, counting the number of the stained pixels darker (i.e. more damaged) than the threshold, and then dividing the area occupied by those pixels by the total wear area. This resulted in a percent of the total area that was damaged, which was used as the metric for wear. To account for the differences in contact areas, the stained contact area was normalized relative to the total specimen area[15]. This method was determined to be sufficiently precise and, due to its executional ease and low cost, a good alternative to the mass analysis. However, since this method does not produce information on the volumetric wear or on the depth profile of the worn surface, it was not deemed sufficiently robust to evaluate cartilage erosion.

Volumetric wear has been measured using nuclear magnetic resonance (NMR) vertical magnet scans of worn cartilage and a curve fitting program that estimated the unworn cartilage surface's topography based on the geometry of the wear track's perimeter[19]. In order to reduce the amount of processing time required by the NMR, as well as to avoid possible error in the curve fitting program, we opted to use a non-contact 3D-scanner. This

enabled a direct comparison of 3D meshes of the cartilage surfaces before and after being worn without risking tissue degradation.

It was recognized that an actual hemiarthroplasty implants with a polished metal surface would be much smoother than the pin surfaces used in the present study. For metal hip components the ASTM F2033-12 standard dictates that surface roughness should not be greater than 50 nm and would probably approach 10 – 25 nm. It is likely that a pin with smooth surfaces in these ranges would wear considerably less in 10,000 cycles than the wear observed in this study. However, testing beyond about 12 hours is not possible in the present test setup because bacterial action would degrade cartilage's mechanical properties. The present simulator accelerated the wear process by using the higher roughness pins in order to allow feasible testing times. Also, the roughness of the stainless steel pins was similar to the roughness of the polymeric pins (tested in Chapter 3), which allowed a comparison of implant materials.

There are limitations associated with using pin-on-plate wear apparatus, as well as with the sort of *in vitro* testing protocol followed by this study. Namely, native geometry and paths of motion are not replicated by the apparatus, and hemiarthroplasty implant finishes were not exactly replicated by the pins. This may have contributed to accelerated wear rates in our testing. However, for the purposes of this comparative study, we deemed the testing protocol sufficient to isolate the independent effect of contact area on wear. Another possible source of error is that physiological processes like inflammatory response that would occur *in vivo* could not be simulated.

While only one load level was examined in this study, it produced stress levels within clinically relevant ranges for various hemiarthroplasty procedures for all of the implant models investigated (Appendix F).

Finally, by varying contact area under a constant load, we could not examine the effect of contact area under the same stress in this study. Further experiments in which different loads are applied by the various hemiarthroplasty implant models in such a way that contact pressure is consistent for each testing condition should be conducted to see

whether volumetric wear and wear track depth increase as steadily as contact area and stress decrease.

2.5 Conclusions

The data suggest that when the hemiarthroplasty contact surface is more conforming and load is distributed over a greater area, less acute cartilage damage occurs. This may be attributed to an improvement in contact mechanics that results from reducing contact stress concentrations between the implant and the cartilage. Fewer differences were observed in net volumetric wear among implant geometries for wear depth than it was for average volumetric wear. This may indicate that the severity of wear is more closely tied to wear depth than it is to the net volume of material lost. As the radii of curvature of the implant models increased, a marked decrease in wear sensitivity was observed which suggests that as implants become rounder, a threshold at which contact mechanics seem to shift detrimentally is reached. The findings of this study prescribe the design of hemiarthroplasty implants with radii of curvature that give the largest contact area and thus the lowest average contact stress to improve their longevity and performance.

2.6 References

1. Gschwend N. Present state-of-the-art in elbow arthroplasty. *Acta Orthop Belg*. 2002;68(2):100-117.

2. Schneeberger AG, Meyer DC, Yian EH. Coonrad-morrey total elbow replacement for primary and revision surgery: A 2-to 7.5-year follow-up study. *Journal of Shoulder and Elbow Surgery*. 2007;16(3):S47-S54.

3. Wright TW, Wong AM, Jaffe R. Functional outcome comparison of semiconstrained and unconstrained total elbow arthroplasties. *Journal of Shoulder and Elbow Surgery*. 2000;9(6):524-531.

4. Burkhart KJ, Nijs S, Mattyasovszky SG, et al. Distal humerus hemiarthroplasty of the elbow for comminuted distal humeral fractures in the elderly patient. *The Journal of Trauma and Acute Care Surgery*. 2011;71(3):635-642.

5. Van Riet RP, Van Glabbeek F, Verborgt O, Gielen J. Capitellar erosion caused by a metal radial head prosthesisA case report. *The Journal of Bone & Joint Surgery Case Connector*. 2004;86(5):1061-1064.

6. Shore BJ, Mozzon JB, MacDermid JC, Faber KJ, King GJ. Chronic posttraumatic elbow disorders treated with metallic radial head arthroplasty. *The Journal of Bone & Joint Surgery*. 2008;90(2):271-280.

7. Van Glabbeek F, Van Riet R, Baumfeld J, et al. Detrimental effects of overstuffing or understuffing with a radial head replacement in the medial collateral-ligament deficient elbow. *The Journal of Bone & Joint Surgery*. 2004;86(12):2629-2635.

8. Liew VS, Cooper IC, Ferreira LM, Johnson JA, King GJ. The effect of metallic radial head arthroplasty on radiocapitellar joint contact area. *Clin Biomech*. 2003;18(2):115-118.

9. McGibbon C, Krebs D, Trahan C, Trippel S, Mann R. Cartilage degeneration in relation to repetitive pressure: Case study of a unilateral hip hemiarthroplasty patient. *J Arthroplasty*. 1999;14(1):52-58.

10. Moon KH, Kang JS, Lee TJ, Lee SH, Choi SW, Won MH. Degeneration of acetabular articular cartilage to bipolar hemiarthroplasty. *Yonsei Med J*. 2008;49(5):719-724. doi: 10.3349/ymj.2008.49.5.719; 10.3349/ymj.2008.49.5.719.

11. Maghen Y, Leo AJ, Hsu JW, Hausman MR. Is a silastic radial head still a reasonable option? *Clinical Orthopaedics and Related Research®*. 2011;469(4):1061-1070.

12. Giannicola G, Sacchetti FM, Antonietti G, Piccioli A, Postacchini R, Cinotti G. Radial head, radiocapitellar and total elbow arthroplasties: A review of recent literature. *Injury*. 2013.

13. Moungondo F, El Kazzi W, van Riet R, Feipel V, Rooze M, Schuind F. Radiocapitellar joint contacts after bipolar radial head arthroplasty. *Journal of shoulder and elbow surgery*. 2010;19(2):230-235.

14. Cruess RL, Kwok DC, Duc PN, Lecavalier MA, Dang GT. The response of articular cartilage to weight-bearing against metal. A study of hemiarthroplasty of the hip in the dog. *J Bone Joint Surg Br*. 1984;66(4):592-597.

15. McGann ME, Vahdati A, Wagner DR. Methods to assess in vitro wear of articular cartilage. *Proc Inst Mech Eng Part H J Eng Med*. 2012;226(8):612-622.

16. Chan S, Neu C, Komvopoulos K, Reddi A, Di Cesare P. Friction and wear of hemiarthroplasty biomaterials in reciprocating sliding contact with articular cartilage. *Journal of tribology*. 2011;133(4).

17. McCann L, Ingham E, Jin Z, Fisher J. An investigation of the effect of conformity of knee hemiarthroplasty designs on contact stress, friction and degeneration of articular cartilage: A tribological study. *J Biomech*. 2009;42(9):1326-1331.

18. McCann L, Udofia I, Graindorge S, Ingham E, Jin Z, Fisher J. Tribological testing of articular cartilage of the medial compartment of the knee using a friction simulator. *Tribol Int*. 2008;41(11):1126-1133.

19. Luo Y, McCann L, Ingham E, Jin Z, Ge S, Fisher J. Polyurethane as a potential knee hemiarthroplasty biomaterial: An in-vitro simulation of its tribological performance. *Proc Inst Mech Eng Part H J Eng Med*. 2010;224(3):415-425.

20. Radin EL, Paul IL. Response of joints to impact loading. I. in vitro wear. *Arthritis & Rheumatism*. 1971;14(3):356-362.

21. Radin EL, Swann DA, Paul IL, Mcgrath PJ. Factors influencing articular cartilage wear in vitro. *Arthritis & Rheumatism*. 1982;25(8):974-980.

22. Forster H, Fisher J. The influence of loading time and lubricant on the friction of articular cartilage. *Proc Inst Mech Eng Part H J Eng Med*. 1996;210(2):109-119.

23. Szarko M, Muldrew K, Bertram JE. Freeze-thaw treatment effects on the dynamic mechanical properties of articular cartilage. *BMC musculoskeletal disorders*. 2010;11(1):231.

24. GE HealthCare HC. Certificate of analysis. . 2012.

25. ISO-14243-3. Implants for surgery: Wear of total knee joint prostheses. part 3: Loading and displacement parameters for wear testing machines with displacement control and corresponding environmental Conditions for test. . 2004.

26. Brandt J. *Wear and boundary lubrication in modular total knee replacements*. 2008.

27. Athanasiou K, Rosenwasser M, Buckwalter J, Malinin T, Mow V. Interspecies comparisons of in situ intrinsic mechanical properties of distal femoral cartilage. *Journal of Orthopaedic Research*. 1991;9(3):330-340.

28. Lizhang J, Fisher J, Jin Z, Burton A, Williams S. The effect of contact stress on cartilage friction, deformation and wear. *Proc Inst Mech Eng Part H J Eng Med*. 2011;225(5):461-475.

29. Bonnevie E, Baro V, Wang L, Burris DL. In situ studies of cartilage microtribology: Roles of speed and contact area. *Tribology letters*. 2011;41(1):83-95.

30. Sathasivam S, Walker PS, Campbell PA, Rayner K. The effect of contact area on wear in relation to fixed bearing and mobile bearing knee replacements. *J Biomed Mater Res*. 2001;58(3):282-290.

Chapter 3

The Effect of Hemiarthroplasty Implant Material on Early *In Vitro* Cartilage Wear

OVERVIEW: *This chapter details a study which examines the effect of Young's modulus (implant stiffness) on early in vitro cartilage wear. Stainless steel, titanium, polyether ether ketone, high density polyethylene, and ultra high molecular weight polyethylene were investigated.*

3.1 Introduction

As mentioned in Chapters 1 and 2, hemiarthroplasty procedures are less surgically invasive and constraining to post-operative range of motion, and preserve more natural bone than total joint arthroplasty. Thus, these implants are a promising alternative for younger, more active patients who may need revision surgeries. However, it has been suggested that the relatively high stiffness of commonly used implant materials is problematic for their long term use due to the decreased articular contact area and increased cartilage stress, which leads to damage of the adjacent articular cartilage[1,2]. *In vivo* studies have reported a correlation between the severity of damage to articular cartilage and the length of time a hemiarthroplasty implant is in place[3-5].Thus, the longevity of hemiarthroplasty implants is limited by wear, which reduces their clinical applicability.

According to the literature, more compliant hemiarthroplasty implant materials may reduce cartilage degeneration [3,6-9], and materials that mimic the biphasic nature of articular cartilage may reduce the coefficient of friction through load sharing to even further reduce wear [10-12]. However, most hemiarthroplasty implants in clinical use are made from cobalt chromium or stainless steel, both of which are approximately 40000 times stiffer than cartilage. Accordingly, 'iso-elastic' materials are being incorporated to hemiarthroplasty implant design, with favorable results in ulnar head hemiarthroplasty in the wrist. When

worn against a simulated bone counterface, CoCr implants produced wear 45 times greater than UHWMPE implants, as measured volumetrically and by penetration depth [13]. Another study showed that alumina, stainless steel, and UHMWPE all produced less cartilage protein loss and a smaller increase in cartilage friction coefficient than CoCr implants [14]. Similarly, an *in vitro* study which isolated the effect of Young's modulus on wear of bovine articular cartilage showed that lower modulus implant models produced less wear than stainless steel hemiarthroplasty; when worn against cartilage in a pendulum friction simulator, three polyeurethane (PU) plates with moduli between 1.4 and 22 MPa wore away significantly less cartilage than a stainless steel plate. Strikingly, the two most compliant polymers produced wear comparable to a cartilage-on-cartilage articulation that was used as a control in the study[9]. Other biocompatible materials that have shown promising wear results include pyrolytic carbon[15,16], poly vinyl alcohol hydrogel[17], ceramics including oxidized zirconium[16,18] and Bionate®[19]. Polyether ether ketone (PEEK), which is currently used as an implant bearing option, is also proposed to be a promising low-modulus implant material, though it has yet to be used in such an application.

It is hypothesized that more compliant implant materials will produce less cartilage wear, but the relationship between implant stiffness and damage to articular cartilage remains unclear. Specifically, whether there is a linear increase in wear as implant stiffness increases, or if there is a threshold level at which contact mechanics shift detrimentally is unknown. Therefore, this study seeks to elucidate the relationship between hemiarthroplasty implant material stiffness and volumetric wear *in vitro* using a pin-on-plate wear simulator. Hemiarthroplasty implant models made from five biocompatible materials with Young's moduli ranging from 0.69 MPa to 200 GPa were reciprocated against semi-confined plugs of bovine articular cartilage. Their performance was evaluated in terms of volumetric wear. As previously stated, we predicted that the softer, more compliant materials would produce less cartilage wear than their stiffer counterparts.

3.2 Materials and Methods

3.2.1 Implant models

Custom made hemispherical-tipped pins with 4.70 mm radii were used as hemiarthroplasty implant models. Two implant models were constructed from each material from cylindrical rods purchased online from McMaster-Carr (www.mcmaster.com; Elmhurst, Illinois, USA). The pins were machined and polished to the desired geometry at University Machine Services at the University of Western Ontario, then soaked in a diluted isopropyl alcohol solution to remove any debris and embedded particles from the surfaces. The average surface roughness of their tips' surfaces were measured using a Tencor P10 surface profilometer (Santa Clara, CA, USA) to ensure that the differences in wear were was not caused by different finishes on the pin surfaces. The materials and properties of the pins are summarized in Table 3-1. No significant differences in the surface roughness were observed among pins ($p>0.05$).

Table 3-1 *Implant material properties*

Implant Material	Young's Modulus [GPa]	Surface Roughness Average, R_a [µm]
Stainless Steel	200	1.9
Titanium	100	1.8
PEEK	3.7	1.2
HDPE	2.7	1.8
UHMWPE	0.69	2.0

Surface roughness (R_a) for typical hemiarthroplasty implants vary between 0.025 µm and 0.25 µm[14,20,21], and the maximum allowable surface roughness average for joint replacement implants is 50nm as per ISO 21534:2007. Since the R_a values of the implant models were higher than these grades, an additional series of wear tests were conducted using geometrically identical silicon nitride (Si_3N_4) tipped pins with 20 nm surface roughness averages. Though this material is not used in orthopedics, this study (the results of which are presented in Appendix C) was conducted to understand the influence of surface roughness on the results.

Scanning electron microscopy was used to image the pins so that their microstructure could be examined. Images of each material were taken at 1000X magnification with 10 kV beam energy using a Hitachi S-4500 Scanning Electron Microscope (Tokyo, Japan). Before scanning, the UHMWPE, PEEK, and HDPE pins were coated in gold.

3.2.2 Tissue Acquisition and Preparation

The tissue acquisition and preparation protocol is similar to that detailed in Chapter 2. Cylindrical cartilage explants were harvested, along with subchondral bone, from the proximal faces of fresh-frozen bovine stifle joints.

Specimens from both the lateral and medial sides of the joint were explanted using a 25 mm diameter diamond-tipped holesaw that bore 5 mm into the bone's surface. For each implant material, four explants each were taken from the lateral and medial side of the joints to randomize the effect of explant provenance. The specimens were potted into custom jigs using Instant Tray Mix (Lang Dental Mfg Co., Inc., Illinois) in such a way that the orientation of the flexion-extension axis of the natural joint would be aligned with the wear piece's path of motion. The cartilage surfaces were then scanned using a non-contact 3D scanner (NextEngine, Santa Monica, California) using the macro range setting, which produces a pointcloud with 0.127 mm accuracy, containing 26 points/mm^2. The pointcloud was exported as a mesh with triangular elements with 0.191 mm edge lengths.

3.2.3 Tribological Simulation

Specimens were worn on a custom six-station pin-on-plate wear simulator in linear reciprocal sliding (Figure 3-1), using the same parameters described in Chapter 2. Eight specimens were worn against each implant material (n=8). The implant models reciprocated against the cartilage plugs at a frequency of 1.2 Hz for a total wear distance of 100 m, under a constant load of 27.5 N.

Specimens were bathed in HyClone™ Alpha Calf Fraction Serum Supplement (ACS; GE Healthcare Life Sciences, Utah, USA) diluted with PBS to a 17 g/L protein concentration and with a 1% Antibiotic-Antimycotic (Invitrogen, Mississauga, ON) concentration for

the duration of testing, as per ISO standards[22]. For the duration of the tribological simulation, a static load was applied to an additional cartilage explant at a 'load soak' station to measure the cartilage's deformation under the load. Penetration depth was measured, then the cartilage was re-submerged in PBS. As in Chapter 2, the worn specimens were submerged in PBS for the duration of time after testing denoted by creep testing detailed in Appendix G to allow the specimens to re-absorb fluid so that the changes observed in the cartilage surface would represent wear, not deformation. This relaxation time was 600 s.

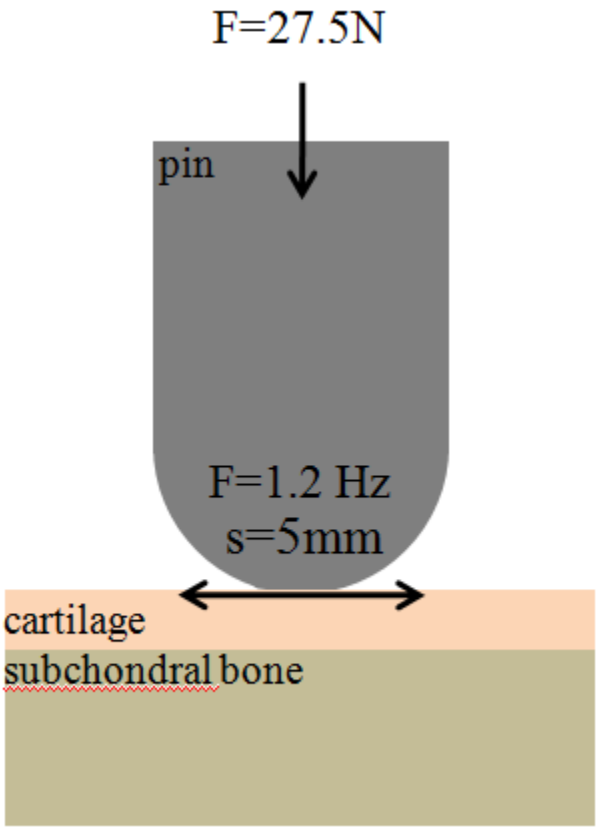

Figure 3-1 *Pin-on-disk wear simulator loading configuration: constant 27.5 N load was applied to the face of the cartilage via the hemiarthroplasty implant model, the pin. This pin reciprocated against the cartilage at a rate 1.2 Hz with a 5 mm stroke length. (Figure previously shown in Chapter 2.)*

An additional six cartilage explants were worn with the very smooth Si_3N_4 tipped pins in the same manner as described above to determine how surface roughness bears on wear and whether the wear observed could be attributed to surface finish. This study is detailed in Appendix C.

3.2.4 Wear Assessment

Wear was assessed using the methodology detailed in Chapter 2, which compares pre- and post-test three dimensional scans of the cartilage surfaces to compute volumetric wear.

For each implant material, eight cartilage plugs were worn. The results are displayed graphically as the mean (n=8) ± standard deviation, and the statistical differences among the groups were analyzed using one way ANOVAs with Kruskal-Wallis multiple comparisons.

3.3 Results

3.3.1 Volumetric Wear

Material loss was observed in all of the specimens. Figure 3-2 shows the volumetric wear for each implant material (mean with standard deviation). The total volume lost was not significantly different among the materials except between PEEK and stainless steel, PEEK and titanium, and PEEK and UHWMPE; with PEEK producing significantly more wear than the other materials ($p<0.05$).

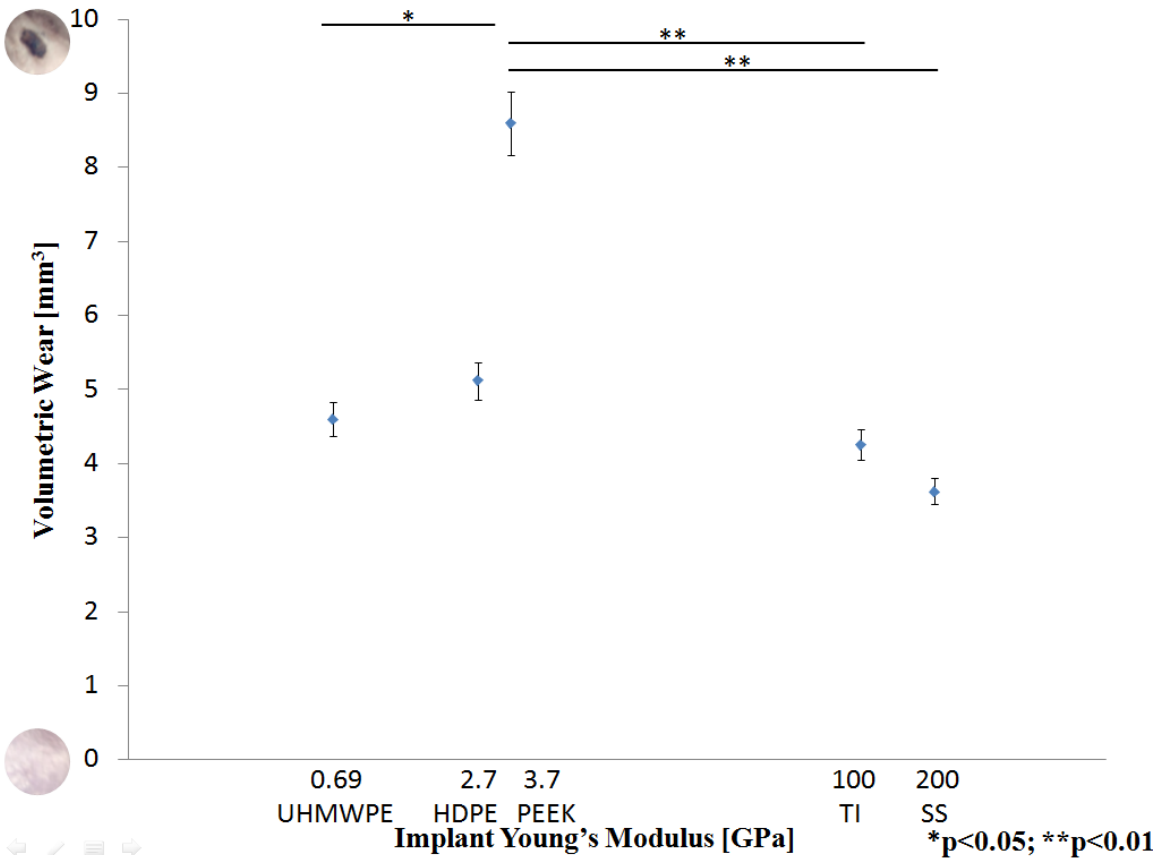

Figure 3-2 *Average volumetric wear for each implant material, with log-scale applied to x-axis. PEEK implants, on average, produced significantly more wear than UHMWPE, TI, and SS implants (*p<0.05; **p<0.01).*

Contrary to our prediction that a decrease in volumetric wear would be observed along with the decrease in implant material stiffness, no trends relating Young's modulus and wear were observed. This indicates that within the range of moduli examined by the study, implant stiffness does not influence wear.

Furthermore, no relationship between the surface roughness average and volumetric wear could be observed in the tested materials. In contrast, the Si_3N_4 pins wore away significantly less material than all of the other implant materials ($p<0.05$), which indicates that for clinical applications, it is absolutely necessary to adhere to the <50nm regulation.

Even so, no other significant differences in wear were associated with the surface finish of the implants (Appendix F).

No discernible trend was observed between roughness average of the pins and volumetric wear. From this we can infer that another material or a chemical property of PEEK leads to an increase in cartilage damage. Figure 3-3 shows a sample of PEEK-worn cartilage stained with India ink to visualize the surface damage qualitatively as compared to a sample worn by a stainless steel pin. Cartilage fibrillation, which has been linked to wear, results in denser pigmentation when stained with India ink[14,23,24].

Figure 3-3 *Comparison of India ink stains: a) Cartilage worn with a stainless steel pin, which shows uniform damage. b) Cartilage worn with a PEEK pin, which shows denser ink pigmentation and increased fibrillation, indicating more severe damage.*

3.3.2 Scanning Electron Microscopy

To determine the effect of microscopic material properties on cartilage wear, scanning electron microscopy (SEM) was conducted. Images taken of an implant of each material by a scanning electron microscope are presented in Figure 3-4 in order to better understand the wear that was observed, particularly the severe wear caused by PEEK, which was neither the stiffest nor the roughest material. The metallic implant models show more uniform surfaces, with machine lines and scratches shown. While all three polymer

implants show crevices and some spall-like surface features, PEEK alone showed deep cracks with over hanging edges, which may have sheared cartilage away, thus accelerating the wear process. The surface asperities of HDPE and UHMWPE both appear directional, but the asperities in the PEEK surface were completely non-uniform and did not appear to follow a machine pattern like those of the other polymers. The depth of the asperities in PEEK may also be conducive to particulate embedding in the surface and degenerative interactions with proteins from the cartilage or from the lubricant.

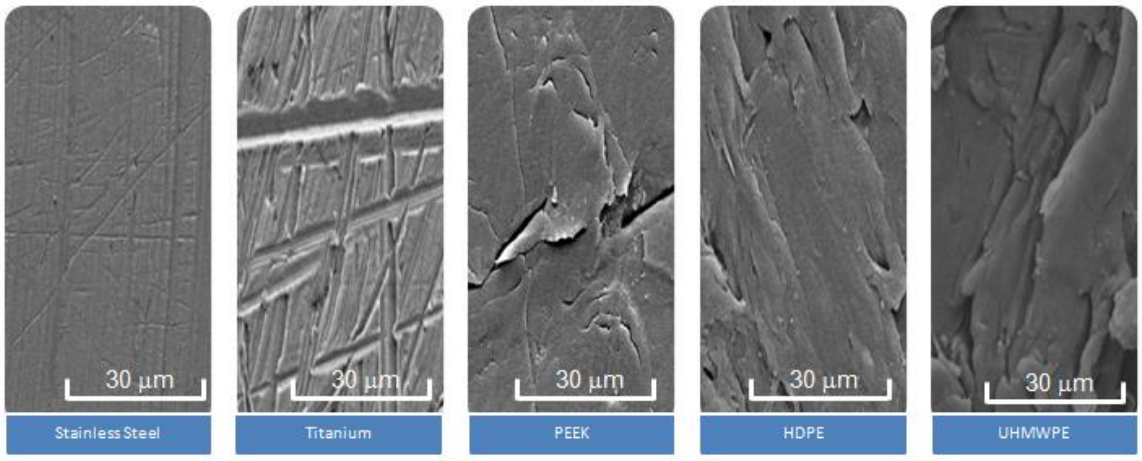

Figure 3-4 *Scanning electron microscopy (SEM) images of an implant of each material taken at 10kV electron beam energy. The PEEK sample shows deep surface asperities with jagged edges which may have contributed the accelerated cartilage wear that was observed.*

3.4 Discussion

The purpose of this study was to elucidate the relationship between hemiarthroplasty implant material stiffness and volumetric wear. It was predicted that more compliant implant materials would produce less wear, and that this study would reveal the stiffness levels at which implant-cartilage contact mechanics deteriorate. However, no such relationship was observed. Among the materials that were examined, PEEK produced the greatest volumetric wear in the cartilage specimens, though its modulus was in the midrange of the group. The most desirable wear results were produced by the stainless

steel pins, which had the highest moduli of the cohort; however, no significant differences in wear were observed among specimens worn with SS and Ti, HDPE, and UHWMPE.

It is inferred from the results of this study that within 0.69 and 200 GPa, stiffness is not the prevailing factor contributing to cartilage wear. This agrees with a study that evaluated cartilage wear caused by various implant materials in terms of friction coefficient, protein assay, and histology conducted by Chan et al. The investigators concluded that CoCr caused more cartilage damage than alumina, SS, and UHMWPE, though it is more compliant than alumina[14]. The softest material examined in this study, UHWMPE, had the most favourable results, but not significantly so.

The previously mentioned study conducted by Luo et al. involved wearing the medial compartments of bovine knees against three polyurethane (PU) plates of varying moduli, a stainless steel plate, as well as a cartilage-on-cartilage control using a pendulum friction simulator[9]. The range of moduli of the PU plates were considerably lower than those investigated by the present study, as well as those investigated by Chan et al. Specifically, they investigated plates with 0.0014 GPa, 0.0065 GPa, and 0.022 GPa moduli. At these lower stiffness levels, the investigators were able to observe significant differences in contact stresses and frictional shear stresses among the SS plate and all of the PU plates, and among the stiffest PU plate and the other two. Notably, no significant difference between the contact stress for the two most compliant PU plates and the cartilage-on-meniscus control were observed[9]. This indicates that the role of implant stiffness in wear is likely more prevalent at lower moduli, approaching the modulus of cartilage.

The role of implant surface finish on volumetric wear was also examined in this study. Surface roughness average measurements taken of the wear pieces revealed that while the pins were much rougher than clinically available hemiarthroplasty implants, the variances in their roughness didn't contribute to the differences in wear that we observed. The results of the surface profilometry indicate that PEEK's relatively poor wear performance could not be attributed to the macro-surface finish, since it had the smoothest finish of the materials tested, though our examination of 20 nm roughness average tipped pins produced significantly less wear than all of the implant models we investigated.

Roughness of implant models has been shown to play a significant role in tissue damage even when the implant models are under the 50 nm ISO standard[25], which agrees with the significant decrease in wear caused by the 20 nm Si3N4 pins relative to all other investigated implant materials. With equally smooth implants (R_a=10 nm) worn against cartilage, Oungoulian et al. observed that stainless steel produced higher levels of wear and friction coefficients than two CoCr alloys[25]. Like in the present study, Oungoulian et al. concluded that implant surface chemistry influences friction coefficient.

While PEEK has shown promise as a potential total arthroplasty implant bearing material because of good wear resistance[26], its use as a hemiarthroplasty material has not been thoroughly evaluated. PEEK has been shown to have high friction coefficients and produce relatively high wear against steel and CoCr though the underlying reasons for the poor surface interactions are largely unknown[27,28]. Our study's results indicate that similar mechanisms are at work at the PEEK-cartilage interface. It is clear that PEEK's material composition contributes to increased friction levels which leads to abrasion in the adjacent material. In the case of cartilage, which is considerably more compliant than PEEK, serious wear is produced.

SEM images taken of each material show that PEEK has deep and irregular surface asperities that may promote spalling in cartilage. Deep cracks with sharp edges were observed in the PEEK implant's surface, which may be shearing into the cartilage, increasing wear and fibrillation. While the SEM images of the UHMWPE also showed sharp asperities, the topography was more uniform than the jagged, deep, isolated asperities seen in the PEEK implant surface. Further examination of PEEK's microstructure, wettability, chemical properties, and interaction with cartilage is necessary to elucidate the mechanisms that contribute to these increased wear rates.

This study, like all *in vitro* studies, does not replicate the clinical conditions in which hemiarthroplasty implants function. Specifically, the pin-on-disk tribometer does not preserve natural joint motion or geometry, the duration of testing was relatively short, and the specimens were harvested from fresh-frozen bovine joints as opposed to live human specimens. For these reasons, significant physiological factors that affect cartilage wear

including inflammatory responses and cellular activity could not be simulated by this study. However, since this study performed a direct comparison of implant materials, it can be deemed adequate as a screening protocol for potential hemiarthroplasty implant materials.

Implant materials that mimic the biphasic nature of articular cartilage may reduce the coefficient of friction through load sharing [10-12] and thus result in less wear than traditional implant materials. Further studies that examine materials with lower moduli, approaching that of articular cartilage, may elucidate a relationship between cartilage wear and implant stiffness.

3.5 Conclusion

The practical implication of this study is that PEEK produces significant wear in articular cartilage; therefore, its use as a hemiarthroplasty implant material should perhaps be discouraged. More generally, within the range of materials examined, Young's modulus, or stiffness, did not have an effect on the wear of articular cartilage. This can perhaps be attributed to the relatively high moduli of the examined materials, which are considerably less complaint than cartilage.

3.6 References

1. Burkhart KJ, Nijs S, Mattyasovszky SG, et al. Distal humerus hemiarthroplasty of the elbow for comminuted distal humeral fractures in the elderly patient. *The Journal of Trauma and Acute Care Surgery*. 2011;71(3):635-642.

2. Maghen Y, Leo AJ, Hsu JW, Hausman MR. Is a silastic radial head still a reasonable option? *Clinical Orthopaedics and Related Research*®. 2011;469(4):1061-1070.

3. Dalldorf PG, Banas MP, Hicks DG, Pellegrini V. Rate of degeneration of human acetabular cartilage after hemiarthroplasty. *The Journal of Bone & Joint Surgery*. 1995;77(6):877-882.

4. Cruess RL, Kwok DC, Duc PN, Lecavalier MA, Dang GT. The response of articular cartilage to weight-bearing against metal.A study of hemiarthroplasty of the hip in the dog.*J Bone Joint Surg Br*. 1984;66(4):592-597.

5. Van Riet RP, Van Glabbeek F, Verborgt O, Gielen J. Capitellar erosion caused by a metal radial head prosthesisA case report. *The Journal of Bone & Joint Surgery Case Connector*. 2004;86(5):1061-1064.

6. Foy JR, Williams PF,3rd, Powell GL, Ishihara K, Nakabayashi N, LaBerge M. Effect of phospholipidic boundary lubrication in rigid and compliant hemiarthroplasty models. *ProcInstMechEng H*. 1999;213(1):5-18.

7. Cook SD, Thomas KA, Kester MA. Wear characteristics of the canine acetabulum against different femoral prostheses. *J Bone Joint Surg Br*. 1989;71(2):189-197.

8. Aigner T, McKenna L. Molecular pathology and pathobiology of osteoarthritic cartilage. *Cellular and Molecular Life Sciences CMLS*. 2002;59(1):5-18.

9. Luo Y, McCann L, Ingham E, Jin Z, Ge S, Fisher J. Polyurethane as a potential knee hemiarthroplasty biomaterial: An in-vitro simulation of its tribological performance. *ProcInstMechEng Part H J Eng Med*. 2010;224(3):415-425.

10. Gleghorn JP, Doty SB, Warren RF, Wright TM, Maher SA, Bonassar LJ. Analysis of frictional behavior and changes in morphology resulting from cartilage articulation with porous polyurethane foams.*Journal of orthopaedic research*. 2010;28(10):1292-1299.

11. Northwood E, Fisher J. A multi-directional in vitro investigation into friction, damage and wear of innovative chondroplasty materials against articular cartilage. *ClinBiomech*. 2007;22(7):834-842.

12. Northwood E, Fisher J, Kowalski R. Investigation of the friction and surface degradation of innovative chondroplasty materials against articular cartilage. *ProcInstMechEng H*. 2007;221(3):263-279.

13. Naidu SH, Radin A. Isoelastic distal ulnar head prosthesis: An<i> in vitro joint simulator study. *J Hand Surg*. 2009;34(3):409-414.

14. Chan S, Neu C, Komvopoulos K, Reddi A, Di Cesare P. Friction and wear of hemiarthroplasty biomaterials in reciprocating sliding contact with articular cartilage. *Journal of tribology*. 2011;133(4).

15. Cook S, Thomas KA, Kester MA. Wear characteristics of the canine acetabulum against different femoral prostheses. *Journal of Bone & Joint Surgery, British Volume*. 1989;71(2):189-197.

16. Jung M, Wieloch P, Lorenz H, et al. Comparison of cobalt chromium, ceramic and pyrocarbonhemiprostheses in a rabbit model: Ceramic leads to more cartilage damage than cobalt chromium. *Journal of Biomedical Materials Research Part B: Applied Biomaterials*. 2008;85(2):427-434.

17. Nakashima K, Sawae Y, Tsukamoto N, Miura H, Iwamoto Y, Murakami T. Wear behaviour of an artificial cartilage material for hemiarthroplasty. . 2010:1169-1172.

18. Patel A, Spector M. Tribological evaluation of oxidized zirconium using an articular cartilage counterface: A novel material for potential use in hemiarthroplasty. *Biomaterials*. 1997;18(5):441-447.

19. Geary C, Jones E, Fitzpatrick D, Kelly CP, Birkinshaw C. In-vitro evaluation of a polyurethane compliant-layer glenoid for use in shoulder arthroplasty. *ProcInstMechEng H*. 2010;224(4):551-563.

20. Atkinson J, Dowson D, Isaac J, Wroblewski B. Laboratory wear tests and clinical observations of the penetration of femoral heads into acetabular cups in total replacement hip joints: III: The measurement of internal volume changes in explanted charnley sockets after 2–16 years in vivo and the determination of wear factors. *Wear*. 1985;104(3):225-244.

21. Laberge M, Dennis Bobyn J, Drouin G, Rivard CH. Evaluation of metallic personalized hemiarthroplasty: A canine patellofemoral model. *J Biomed Mater Res*. 1992;26(2):239-254.

22. ISO-14243-3. Implants for surgery: Wear of total knee joint prostheses. part 3: Loading and displacement parameters for wear testing machines with displacement control and corresponding environmental Conditions for test. . 2004.

23. Athanasiou K, Rosenwasser M, Buckwalter J, Malinin T, Mow V. Interspecies comparisons of in situ intrinsic mechanical properties of distal femoral cartilage. *Journal of Orthopaedic Research*. 1991;9(3):330-340.

24. McGann ME, Vahdati A, Wagner DR. Methods to assess in vitro wear of articular cartilage. *ProcInstMechEng Part H J Eng Med*. 2012;226(8):612-622.

25. Oungoulian SR, Durney KM, Jones BK, Ahmad CS, Hung CT, Ateshian GA. Wear and damage of articular cartilage with friction against orthopedic implant materials. *J Biomech*. 2015.

26. Stolarski T. Tribology of polyetheretherketone. *Wear*. 1992;158(1):71-78.

27. Schroeder R, Torres F, Binder C, Klein A, de Mello J. Failure mode in sliding wear of PEEK based composites. *Wear*. 2013;301(1):717-726.

28. Scholes S, Unsworth A. Wear studies on the likely performance of CFR-PEEK/CoCrMo for use as artificial joint bearing materials. *J Mater Sci Mater Med*. 2009;20(1):163-170.

Chapter 4

The Effect of Hemiarthroplasty Implant Geometry and Material on Contact Mechanics: A Finite Element Analysis

OVERVIEW: *This chapter expounds a finite element simulation conducted to eludicate relationships among stress levels at the implant-cartilage interface and the in vitro wear results presented in Chapter 2 and Chapter 3.*

4.1 Introduction

Finite element modeling is frequently employed in orthopedic biomechanics to predict contact area, contact pressure, and stress distributions for both intact and replaced joints. These methods are often more accurate for parametric evaluations than *in vitro* measurement techniques, and do not require intervention to quantify contact mechanics[1]. Further, by discretizing the surface geometry of anatomical structures, site-specific material properties can be implemented into models to provide a detailed, comprehensive account of articular contact mechanics at any given point on the surface.

Articular cartilage has been most accurately modeled as an anisotropic, biphasic material in many finite element simulations[2-4], and, in the context of hemiarthroplasty, the time dependence of cartilage contact mechanics has been demonstrated using FEA[5]. However, simpler models which reduce the computational expense of biphasic models have been equally well-reported in the literature[6-13]. These models assign a single, non-linear phase to the cartilage in accordance with hyperelastic laws. Similarly, subchondral bone models based on three-dimensional computed tomography reconstructions account for the non-homogenous properties of bone.

These simulations have been used to complement *in vitro* wear studies by determining stress levels which are then related to experimental wear results[14,15]. As such, a finite element simulation was conducted to provide more insight on the implant-cartilage

interaction by correlating the *in vitro* wear results of Chapters 2 & 3 to articular stress levels.

4.2 Materials and Methods

A simplified, two-dimensional axisymmetric model constructed in Abaqus v6.12-2 (Simula Corp., Providence, RI, USA) simulated the static loading of cartilage explants for each implant geometry (the five implant models with radii of curvature ranging from 4.70 mm to 11.7 mm) and materials (stainless steel, titanium, PEEK, HDPE, and UHMWPE) that were investigated. Contact area, average and peak contact stresses, and penetration depth were measured under a constant load of 27.5 N. The model had a 1:1 scale ratio.

4.2.1 Implant Models

For the investigation of the effect of contact area by varying geometry, the implant models were assigned the material properties of stainless steel with 200 GPa stiffness and a Poisson's ratio of 0.28. Their radii of curvarture varied as shown in Figure 4-1 so that for each contact geometry, stress levels at the implant-cartilage interface could be extracted. The pins were meshed using tetrahedral elements with an average global edge length of 0.05 mm.

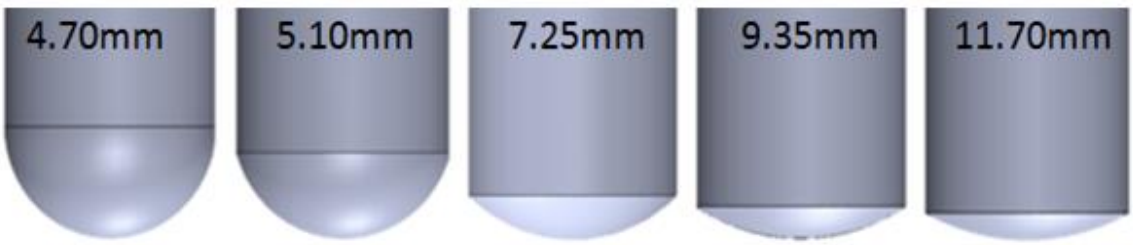

Figure 4-1 *Implant geometries modeled. E=200 GPa, v=0.28 (figure previously presented in Chapter 2).*

To investigate the effect of varying material stiffness on contact mechanics, the implant models, whose Young's moduli and Poisson's ratios were varied to simulate each tested material, were meshed with tetrahedral elements with average global edge lengths of 0.05

mm. Table 4-1 shows the materials with their corresponding properties, and Figure 4-2 shows the models of the implants.

Table 4-1 *Implant Material Properties*

Implant Material	Young's Modulus [GPa]	Poisson's Ratio
Stainless Steel (SS)	200	0.28
Titanium (Ti)	100	0.36
PEEK	3.7	0.36
HDPE	2.7	0.42
UHMWPE	0.69	0.49

Figure 4-2 *Implant models, in order of descending Young's Modulus.*

4.2.2 Cartilage and Bone Models

A neohookean hyperelastic model was assigned to simulate the mechanical response of cartilage in equilibrium. Three layers of linear quadrilateral mesh with global average edge lengths of 0.05 mm were used to model the cartilage layer, shown in Figure 4-3. The mesh geometry allowed for compression of the elements without reducing their volume, and a convergence study deemed the element size sufficiently fine. Cartilage was assigned a Young's modulus of 10 MPa and a Poisson's ratio of 0.4[2,6,16,17].

Bone was modeled using an elastic material model with a Young's modulus of 109MPa and a Poisson's ratio of 0.3[18]. The bone was meshed using linear quadrilateral elements with a 0.1 mm edge length.

The cartilage was assigned a thickness of 2.5 mm, as per experimental measurement. The cartilage model consisted of 1200 linear quadrilateral elements, the bone model consisted of 10000 linear quadrilateral elements, and the pin consisted of 16434 linear quadrilateral elements and 515 linear triangular elements. The two dimensional model therefore had 56298 degrees of freedom. All mesh sizes were deemed adequate by mesh convergence studies.

4.2.3 Boundary and Loading Conditions

An assembly was constructed from the cartilage model and the subchondral bone model. The two parts were mated using a rigid pin constraint, and was constrained axially and rotationally. The motion of the pin was also constrained axially and rotationally, but allowed to move in the plane perpendicular to the face of the cartilage-subcondral bone assembly. A concentrated force of 27.5 N was applied in this direction (along the superior-inferior y-axis) to the pin model, against the face in the cartilage as in the *in vitro* tests.

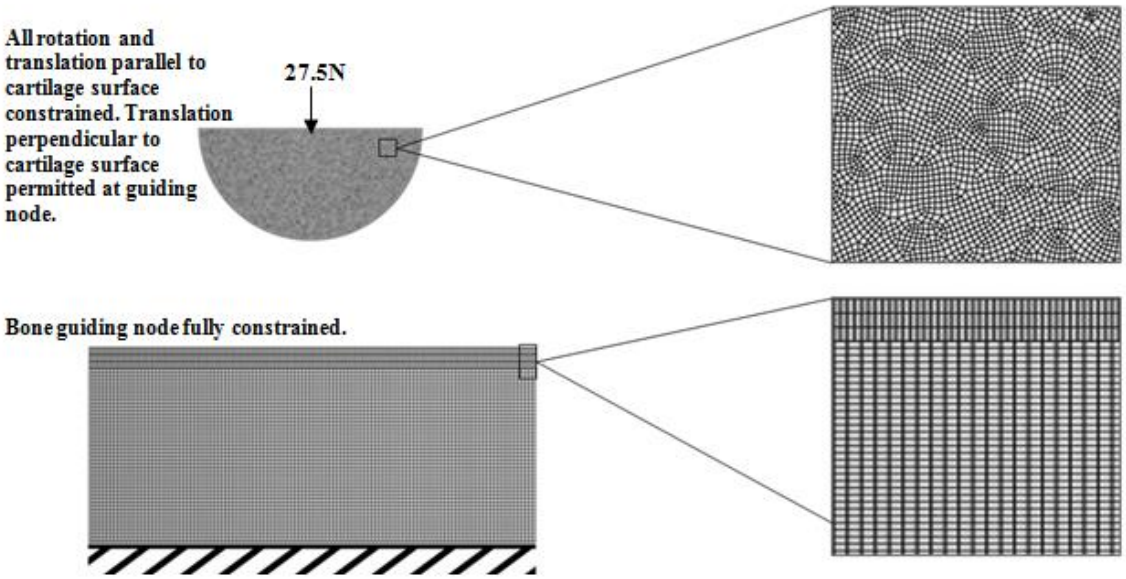

Figure 4-3 *Boundary conditions and meshes for finite element models.*

4.2.4 Measurement Regions and Output Variables

Data were extracted from nodes in the cartilage layer to determine contact mechanics. The output variables were contact displacement, contact nodal area, and contact stresses.Contact area was determined from the region between nodes in which the contact pressure was greater than zero. Peak von Mises contact stresses were quantified along with the contact stress at certain regions of interest. Additionally, the diameter of the region of cartilage subjected to the peak contact stress and the maximum penetration depth of the pin into the cartilage were measured.

4.2.5 Model Validation

The model was validated by comparing the contact area at the implant-cartilage interface to those measured using a reproducible casting technique[19-21]. Silicone-based dental cement, Reprosil® (Dentsply International Inc., Milford, DE, USA) was allowed to cure between the implant and the cartilage under compressive loading, which were fixed using a custom-made jig. Contact area was measured using MicroScribe 3D Digitizer and its software utility package (Immersion Inc., San Jose, California, USA) by digitizing the area from which the casting material was pressed out of the articulation. A custom MATLAB (The MathWorks, Inc., Natick, Massachusetts, USA) program calculated the area occupied by the resultant point cloud (included in Appendix H). For each material, two casts were taken and the contact area measurements were repeated three times and averaged to reduce error.

Additionally, the FEA results were further validated by directly measuring contact area using pressure-sensitive film. Pressure Sensitive Film® (Fujifilm Holdings Corporation, Tokyo, Japan) has been used to measure contact pressure and contact area in many biomechanical investigations[22-24]. In the static load soak station, the film was inserted directly between the implant and the cartilage surface. The film was left in place for the amount of time that the specimens took to reach the wear distance (139 minutes). The film was removed, and then analyzed using Topaq Pressure Analysis System (Sensor Products Inc, Madison, NJ, USA). This was repeated for each implant geometry and material. The

contact area from the casting technique, the pressure-sensitive film, and the FEA outcomes were compared for all implant geometries and implant materials.

4.3 Results

Figure 4-4 compares the contact area measured from casts taken of the cartilage-implant model interface and the contact area measurements from the Fuji Film Pressure Sensitive Film® with the contact area estimated by the finite element simulation for the 5.1 mm implant model. The exact values are provided in Appendix I.

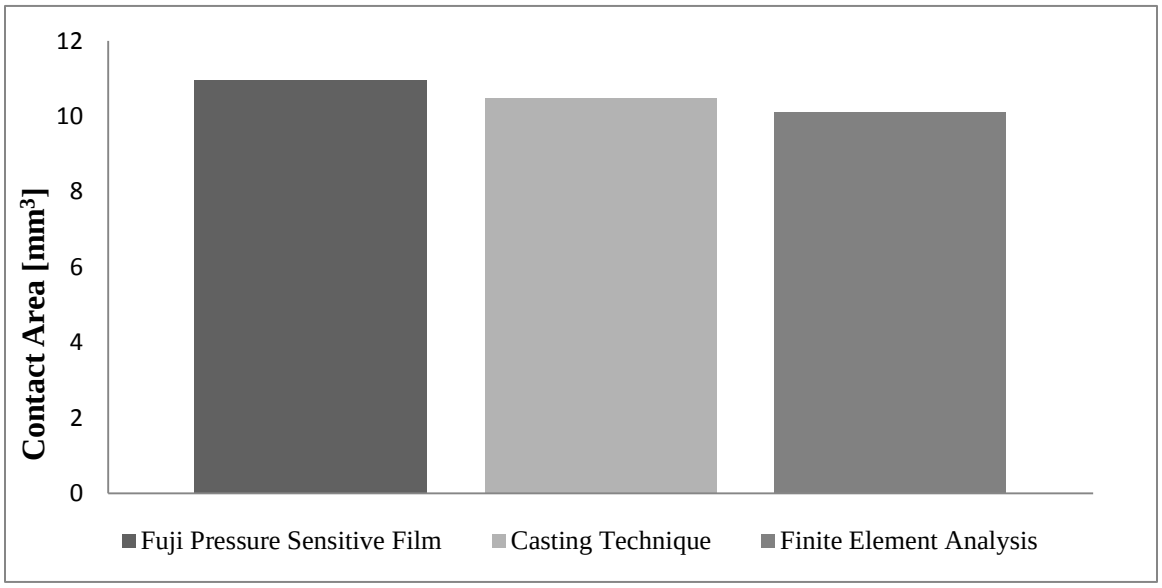

Figure 4-4 *Comparison of contact area measurements from casting, pressure-sensitive film, and finite element analysis for the ROC=5.10mm implant model.*

As illustrated, the experimental values and the theoretical predictions agree rather well, under 10% in the worst case, which was between the measurements taken with the Film Pressure Sensitive Film® and the FEA. The FEA peak von Mises (VM) stress, peak contact pressure, maximum penetration depth, and the diameter of the region subjected to peak contact von Mises stress are summarized in TABLE 4-2, and displayed graphically in Figure 4-5.

Table 4-2 *Summary of FEA Results for Varying Implant Geometry*

Tip ROC [mm]	Peak VM Stress [MPa]	Peak Contact Pressure [MPa]	Maximum Penetration Depth [mm]	Diameter of peak VM stress [mm]
4.70	13.4	13.8	0.321	0.75
5.10	12.2	12.7	0.308	0.75
7.25	10.9	11.5	0.283	0.89
9.35	9.46	10.4	0.268	0.89
11.7	8.72	9.52	0.255	1.1

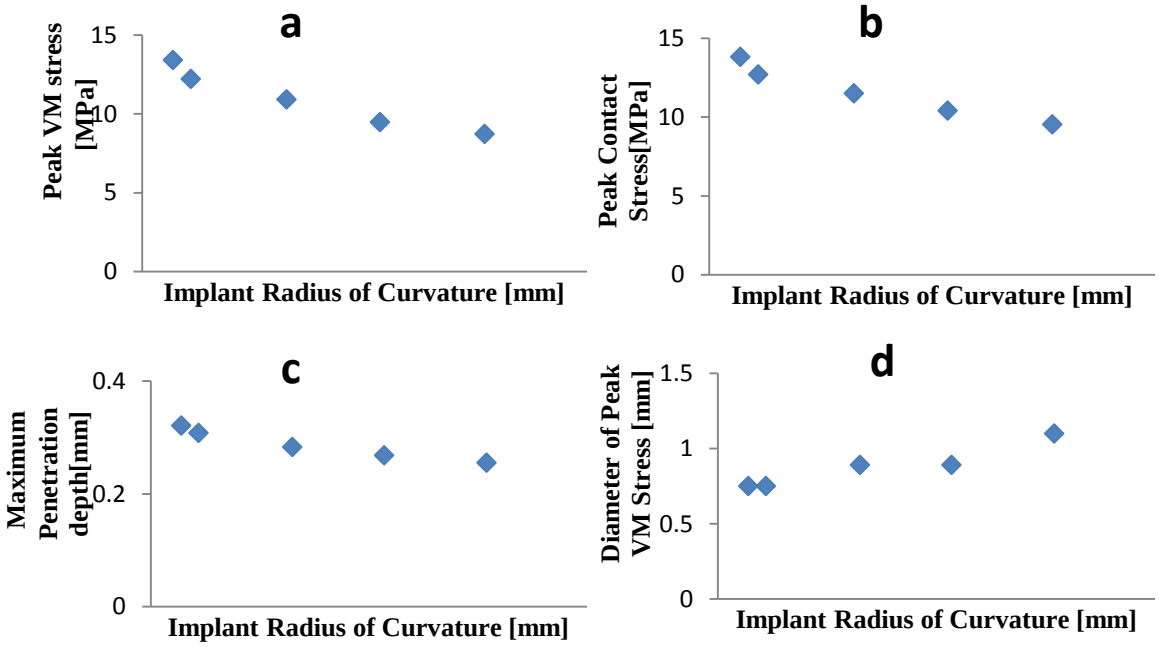

Figure 4-5 *Summary of FEA Results: a) Peak VM Stress in cartilage; b) Peak Contact Stress at the interface; c) Maximum penetration depth; d) diameter of maximum VM stress region, all as a function of implant radius of curvature.*

Figure 4-6 shows the peak Von Mises stress distributions for each of the tip geometries, which reduces gradually as the radius of curvature of the implant increases.

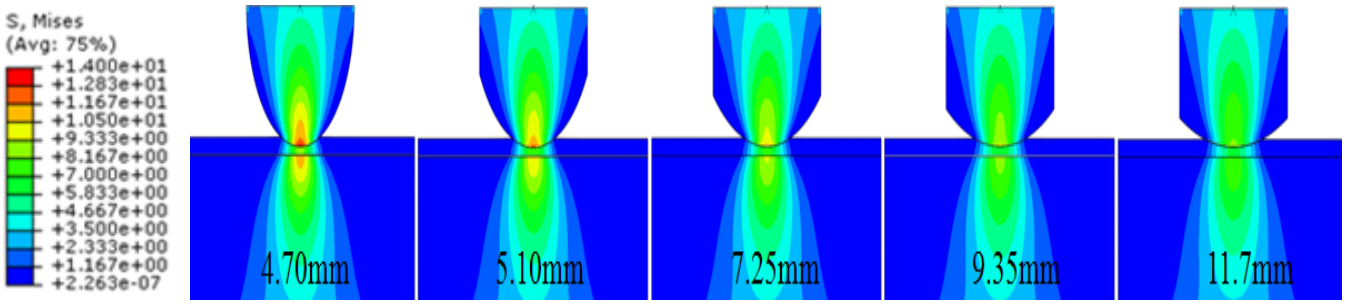

Figure 4-6 *Von Mises Stress distributions along implant-cartilage interface in order of increasing radius of curvature.*

Conversely, no differences in peak stress, contact area, or penetration depth were observed among the material models, as shown in Table 4-3, which summarizes FEA peak von Mises (VM) stress, peak contact pressure, maximum penetration depth, and the diameter of the region subjected to peak contact von Mises stress. Figure 4-7 graphically depicts the same results.

Table 4-3 *Summary of FEA Results for Varying Material*

Tip Material	Peak VM Stress [MPa]	Peak Contact Pressure [MPa]	Maximum Penetration Depth [mm]	Diameter of peak VM stress [mm]
SS	13.4	13.8	0.321	0.75
Ti	13.4	13.8	0.321	0.75
PEEK	13.4	13.8	0.321	0.75
HDPE	13.4	13.8	0.321	0.75
UHMWPE	13.4	13.8	0.321	0.75

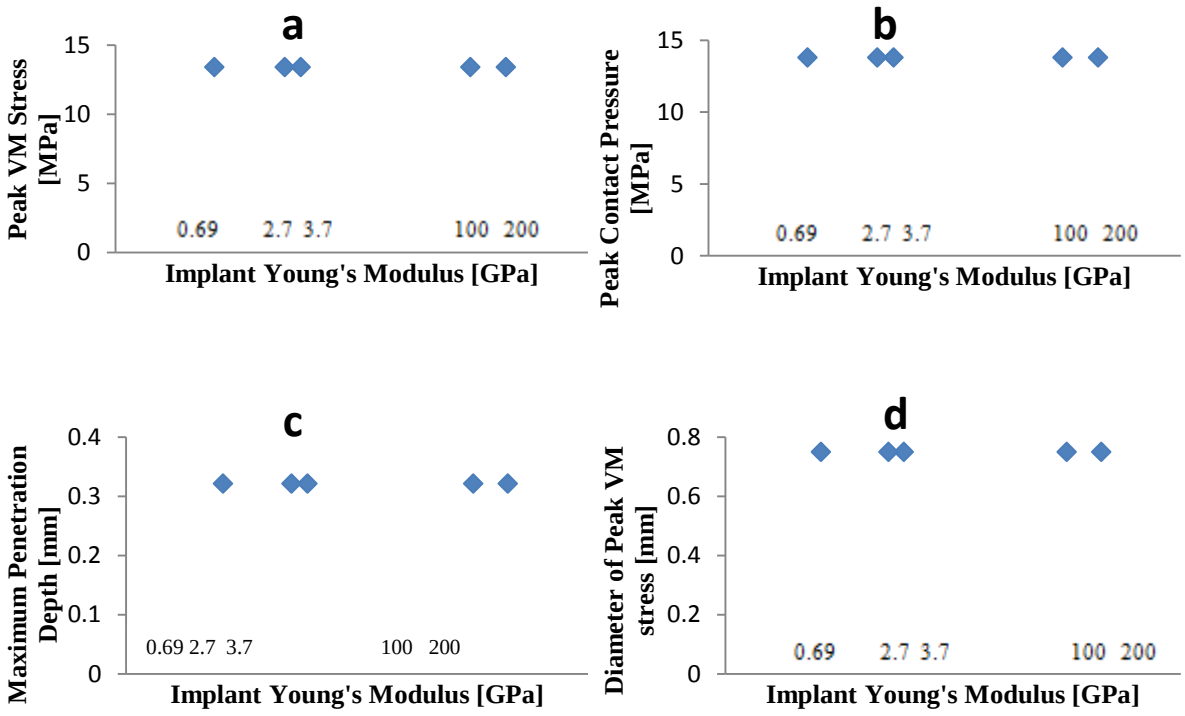

Figure 4-7 *Summary of FEA Results: a) Peak VM Stress in cartilage; b) Peak Contact Stress at the interface; c) Maximum penetration depth; d) diameter of maximum VM stress region, all as a function of implant Young's modulus. Note: A logarithmic scale was applied to the x-axis.*

4.4 Discussion

The finite element simulation for varying geometry was conducted to understand the relationship between the wear that was observed to stress levels at the cartilage-implant model interface. The agreement between the measured contact area and the simulation's estimations of contact area indicate that the model is an accurate representation of the contact mechanics during the *in vitro* wear simulation.

A two-dimensional model was constructed to simulate the loading configuration of the pin-on-disk tribometer. This idealization saved on the computational expense of a three dimensional finite element simulation while preserving the integrity of results. Cilngir et al. compared the contact mechanics of a three FEA models of a hip hemiarthroplasty to

determine whether utilizing three dimensional, anatomical models was worth the computational time[25]. Between a three dimensional anatomical model and a two dimensional axisymmetric model, a difference of only 7% in the maximum von Mises stresses was observed. The investigators therefore concluded that two dimensional models can be used to determine contact mechanics at hemiarthroplasty implant-cartilage articulations.

The general trend observed by the FEA supports the broad findings of Chapter 2: namely, that increasing contact area has a beneficial effect on implant-cartilage contact mechanics. Results reported Büchler et al., who conducted an FEA study that examined the influence of shape of shoulder hemiarthroplasty implants[26] support our finding that maximizing contact area at the cartilage-implant articulation is critical to stress reduction. An intact shoulder model was compared to shoulder models reconstructed with two humeral head hemiarthroplasty implants: a 'second generation' Neer II humeral component (Smith & Nephew, Inc., Memphis, Tennessee, USA), and an anatomically reconstructed humeral head. The investigators found that the more congruent anatomical implanted model and the intact model had similar contact area locations, peak VM stresses, and contact pressures for various loading orientations. However, the second generation implant produced shifted contact areas, and in certain orientations, up to a nearly 700% increase in peak VM stresses.

The possible stress thresholding phenomenon that was observed in Chapter 2's *in vitro* study was also supported by the FEA. Between ROC= 4.7 mm and ROC=7.25 mm, the rate at which stress increased was considerably higher than among the other ROC intervals, as shown in Figure 4-8, which shows peak VM stress as a function of ROC above the volumetric wear results from Chapter 2. The slopes of the highlighted segments are shown to emphasize the changes in stress sensitivity that were observed as ROC increased, specifically, at lower ROC, stresses were highly dependent on ROC, but that at lower ROC, stresses were fairly insensitive to ROC. While the disparity in the rates of changes is greater for volumetric wear than it is for stresses, the decrease in stresses shown by the FEA seemed to produce a proportional decrease in wear. This indicates that the decrease in wear's sensitivity to radius of curvature may be related to stress, and

supports the suggestion made in Chapter 2 that between ROC=9.35 mm and ROC=7.25 mm a detrimental shift in contact mechanics occurs.

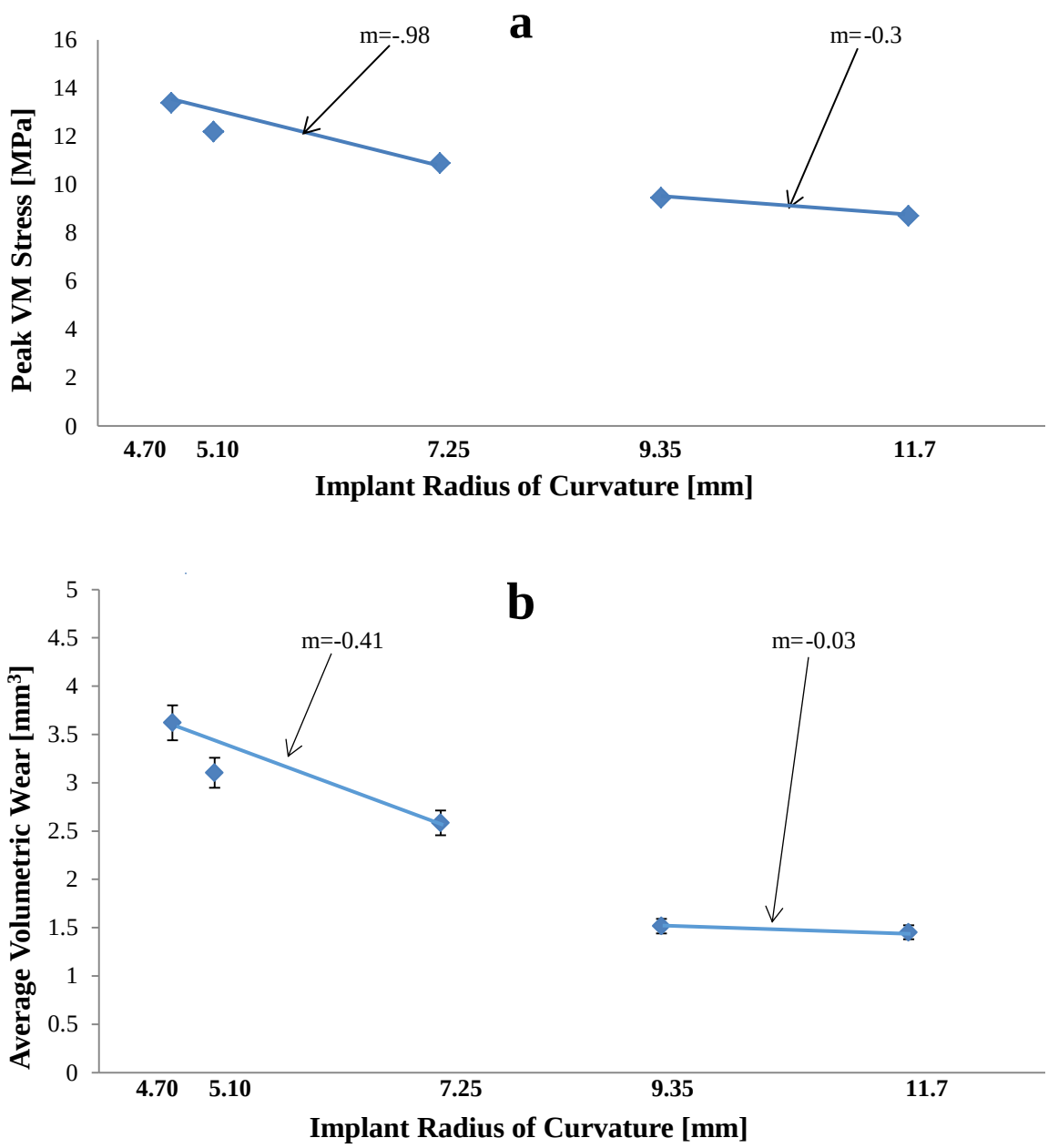

Figure 4-8 *a) FEA Peak von Mises Stress as a Function of radius of curvature (ROC) with slopes between segments shown. b) Average volumetric wear results as a function of radius of curvature. As ROC increased, stresses became less sensitive to changes ROC, which may explain the reduction in wear's sensitivity to ROC for the flatter implant models shown in b).*

The critical failure stress for articular cartilage has been shown to range from 15- 30 MPa. This range of stresses has been associated with the mechanical failure in the form of cracks in cartilage explants, as well as in chondrocyte death, which has been shown to precede tissue degeneration[27,28]. The increased wear rates that we noted for the 4.70 mm and 5.10 mm ROC pins could also be explained by the fact that the stress levels imposed on the cartilage (as determined by the FEA) approach 14 MPa, which is very close to the lower end of this ultimate failure range.

Interestingly, no effect of implant modulus on any of the examined variables was observed. This indicates that within the range of moduli that were investigated, that compliance did not increase enough to increase articular contact area and reduce contact stress. The lack of a stress-to-material trend accords well with the *in vitro* wear results for all materials except for PEEK. This supports the hypothesis that the high wear caused by the PEEK implants is not related to contact mechanics (stress), but to frictional or chemical interactions.

Stress levels on the native bovine elbow have been shown to be 0.82 MPa in compression[29]. Stress levels imposed on the cartilage specimens in our study were higher than those of the native bovine elbow, but, as previously mentioned, the reduction in articular contact area following hemiarthroplasty procedures leads to an increase in contact stress.

The results of this analysis investigating material stiffness showed no differences in contact stresses among implant materials, and agree with the results of the *in vitro* wear tests conducted in Chapter 3. A similar FEA study conducted to investigate the role of material selection on cartilage stress following partial joint replacements in the shoulder joint found similar results; among CoCr, TI, pyrolytic carbon, and PEEK, no significant differences in cartilage stresses were observed[30]. As concluded in Chapter 3, this suggests that if an implant's Young's modulus has a discernible effect on cartilage contact mechanics, it likely occurs at moduli well below 0.69GPa.

4.5 Conclusion

The increase in stress levels shown by the FEA accord well with the *in vitro* results in Chapter 2, which indicates that the increase in volumetric wear and wear track depth could be reasonably attributed to the increase in contact stress caused by the reduction in articular contact area for the implants with lower radii of curvature (ROC= 4.70 mm, ROC=5.10 mm, and ROC=7.25 mm). Furthermore, for the implants with larger radii of curvature (ROC=9.35 mm and ROC=11.7 mm), the decrease in contact area and stresses observed accorded well with the wear results which showed a negligible decrease in wear as radius of curvature increased. This indicates that between ROC=7.25 mm ROC=9.35 mm, a threshold at which stresses become less sensitive to ROC is reached.

Within the range of implant material moduli that was examined, no differences in stress levels or distributions were observed in the FEA models. From this, we can conclude that the differences in wear observed among materials in Chapter 3 cannot be attributed to implant stiffness. This supports the hypothesis that more complex surface interactions are at work at the implant-cartilage interface, particularly between PEEK and cartilage.

As in any finite element simulation, approximations of material properties and behaviour under loading conditions were made. The material properties assigned to the models were taken from the literature as opposed to from direct measurement. Though both the solid and fluid constituents of cartilage distribute loads, as in any biphasic poroelastic medium, this model only accounts for the bulk properties of cartilage and neglects the effect of fluid flow though the medium. Furthermore, this FEA study did not account for the time dependent behaviour of cartilage in the loading scenario.

4.6 References

1. Winby CR, Lloyd DG, Besier TF, Kirk TB. Muscle and external load contribution to knee joint contact loads during normal gait. *J Biomech*. 2009;42(14):2294-2300.

2. Goldsmith A, Hayes A, Clift SE. Application of finite elements to the stress analysis of articular cartilage. *Med Eng Phys*. 1996;18(2):89-98.

3. Clift SE. Finite-element analysis in cartilage biomechanics. *J Biomed Eng*. 1992;14(3):217-221.

4. Huiskes R, Chao E. A survey of finite element analysis in orthopedic biomechanics: The first decade. *J Biomech*. 1983;16(6):385-409.

5. Manda K, Eriksson A. Time-dependent behavior of cartilage surrounding a metal implant for full-thickness cartilage defects of various sizes: A finite element study. *Biomechanics and Modeling in Mechanobiology*. 2012;11(5):731-742.

6. Büchler P, Ramaniraka N, Rakotomanana L, Iannotti J, Farron A. A finite element model of the shoulder: Application to the comparison of normal and osteoarthritic joints. *Clin Biomech*. 2002;17(9):630-639.

7. Anderson AE, Ellis BJ, Maas SA, Weiss JA. Effects of idealized joint geometry on finite element predictions of cartilage contact stresses in the hip. *J Biomech*. 2010;43(7):1351-1357.

8. Pistoia W, Van Rietbergen B, Lochmüller E, Lill C, Eckstein F, Rüegsegger P. Estimation of distal radius failure load with micro-finite element analysis models based on

three-dimensional peripheral quantitative computed tomography images. *Bone*. 2002;30(6):842-848.

9. Bendjaballah MZ, Shirazi-Adl A, Zukor D. Finite element analysis of human knee joint in varus-valgus. *Clin Biomech*. 1997;12(3):139-148.

10. Lan C, Xiuli D, Yutao Z, et al. Finite element analysis of LTI carbon hip joint head. 2009:1-4.

11. Friedman RJ, LaBerge M, Dooley RL, O'Hara AL. Finite element modeling of the glenoid component: Effect of design parameters on stress distribution. *Journal of Shoulder and Elbow Surgery*. 1992;1(5):261-270.

12. Anderson AE, Ellis BJ, Maas SA, Peters CL, Weiss JA. Validation of finite element predictions of cartilage contact pressure in the human hip joint. *J Biomech Eng*. 2008;130(5):051008.

13. Willing RT, Lalone EA, Shannon H, Johnson JA, King GJ. Validation of a finite element model of the human elbow for determining cartilage contact mechanics. *J Biomech*. 2013;46(10):1767-1771.

14. McGann ME, Vahdati A, Wagner DR. Methods to assess in vitro wear of articular cartilage. *Proc Inst Mech Eng Part H J Eng Med*. 2012;226(8):612-622.

15. Li L, Patil S, Steklov N, et al. Computational wear simulation of patellofemoral articular cartilage during< i> in vitro testing. *J Biomech*. 2011;44(8):1507-1513.

16. Kempson GE. Mechanical properties of articular cartilage. *J Physiol*. 1972;223(1):23P.

17. Büchler P, Ramaniraka N, Rakotomanana L, Iannotti J, Farron A. A finite element model of the shoulder: Application to the comparison of normal and osteoarthritic joints. *Clin Biomech*. 2002;17(9):630-639.

18. Hayes WC, Bouxsein M. Biomechanics of cortical and trabecular bone: Implications for assessment of fracture risk. *Basic orthopaedic biomechanics*. 1991;2:69-111.

19. Stormont T, An K, Morrey B, Chao E. Elbow joint contact study: Comparison of techniques. *J Biomech*. 1985;18(5):329-336.

20. Liew VS, Cooper IC, Ferreira LM, Johnson JA, King GJ. The effect of metallic radial head arthroplasty on radiocapitellar joint contact area. *Clin Biomech*. 2003;18(2):115-118.

21. Lalone EA, McDonald CP, Ferreira LM, Peters TM, King GW, Johnson JA. Development of an image-based technique to examine joint congruency at the elbow. *Comput Methods Biomech Biomed Engin*. 2013;16(3):280-290.

22. Bachus KN, DeMarco AL, Judd KT, Horwitz DS, Brodke DS. Measuring contact area, force, and pressure for bioengineering applications: Using fuji film and TekScan systems. *Med Eng Phys*. 2006;28(5):483-488.

23. Fregly BJ, Sawyer WG. Estimation of discretization errors in contact pressure measurements. *J Biomech*. 2003;36(4):609-613.

24. Drewniak EI, Crisco JJ, Spenciner DB, Fleming BC. Accuracy of circular contact area measurements with thin-film pressure sensors. *J Biomech*. 2007;40(11):2569-2572.

25. Cilingir A, Ucar V, Kazan R. Three-dimensional anatomic finite element modelling of hemi-arthroplasty of human hip joint. *Trends Biomater Artif Organs*. 2007;21(1):63-72.

26. Büchler P, Farron A. Benefits of an anatomical reconstruction of the humeral head during shoulder arthroplasty: A finite element analysis. *Clin Biomech*. 2004;19(1):16-23.

27. Finlay, J. B., & Repo, R. U. (1977). Impact characteristics of articular cartilage.*ISA transactions*, *17*(1), 29-34.

28. Torzilli, P. A., Grigiene, R., Borrelli, J., & Helfet, D. L. (1999). Effect of impact load on articular cartilage: cell metabolism and viability, and matrix water content. *Journal of biomechanical engineering*, *121*(5), 433-441.

29. Simon WH. Scale effects in animal joints. I. articular cartilage thickness and compressive stress. *Arthritis & Rheumatism*. 1970;13(3):244-255.

30. Reeves J, Razfar N, Langohr G, Athwal G, King G, Johnson J. The effect of material selection and implant positioning on cartilage stresses following partial joint resurfacing: A finite element study. *Orthopaedic Research Society Annual Meeting*. 2015(Montreal, Quebec).

Chapter 5

Overall Conclusions and Future Research Directions

This work was conducted to establish a simple, effective protocol to quantify cartilage wear and to supplement the limited understanding of hemiarthroplasty contact mechanics. The specific objectives outlined at the outset of this work have been fulfilled with some data that support hypothetical predictions as well as some unexpected results. These objectives include the following:

1. To develop an efficient and effective alternative to traditional methods of quantifying cartilage wear.
2. To quantify the effects of varying implant-cartilage contact area on cartilage damage.
3. To elucidate the effects of varying implant material on cartilage wear.
4. To relate *in vitro* wear results with cartilage stress levels using finite element analysis.

The hypotheses and findings of the studies detailed in Chapters 2, 3, and 4, which sought to fulfill these objectives, are reviewed and summarized below.

5.1 Three Dimensional Scanning Protocol for the Measurement of Cartilage Wear

Chapter 2 and Appendix B detail a novel methodology for the quantification of cartilage wear. It was proposed that the methodological stringency of traditional wear measurement procedures could be avoided without compromising scientific rigour using high-precision 3-D scans of the cartilage surface. The protocol that was developed proved to be time-effective, which promoted the heuristic fecundity of the studies that were performed. Specimen preparation guidelines were examined to conclude that fresh-frozen bovine cartilage samples could be used instead of fresh specimens, which enabled the procurement of more samples and alleviated some of the time-sensitivity involved with explanting fresh samples.

The use of a three dimensional scanner enabled the rapid and accurate capture of detailed three dimensional meshes that represent the cartilage surface before and after the tribological simulation so that a direct comparison of the cartilage topography could be conducted without risking additional tissue degeneration. The India ink staining protocol supplemented the data with qualitative insights on cartilage damage.

Further validation of the methodology used wherein volumetric wear measurements taken from 3D scanning are directly compared to wear measured by measuring the protein content of the lubricating bath after testing or compared to mass changes in the cartilage explants are necessary to draw conclusions on net wear, but as a comparative, implant property screening protocol, the methods detailed are promising.

5.2 The Effect of Implant Contact Radius on Cartilage Wear

As predicted, the study detailed in Chapter 2 concluded that greater articular contact area has a beneficial effect on contact mechanics, as demonstrated by reduced volumetric wear. Significantly more cartilage was removed from the surfaces of cartilage worn by the implants with smaller radii of curvature as compared to the more planar implants. More severe fibrillation and deeper wear tracks were also observed among these specimens. Interestingly, average wear depth increased at a greater rate than net volumetric wear as implant radius of curvature decreased. This, coupled with the increase in fibrillation, indicates that more severe cartilage wear was caused by the lower radius of curvature tipped pins.

The disparity between the rate increase of volumetric wear and wear depth may be explained by a more thorough characterization of cartilage wear. As mentioned in the previous section, a histological examination of the cartilage surface, and measurement of the protein content of the lubricating bath after wear may provide a more thorough account of the damage that was induced.

An apparent threshold was observed where cartilage wear and wear depth became insensitive to the radius of curvature. As the implant models became flatter, the

differences in their radii did not contribute to their wear performance, whereas in the rounder tipped pins, significant increases in wear were observed as radius decreased.

5.3 The Effect of Implant Stiffness on Cartilage Wear

Contrary to the hypothesis that more compliant implant materials would produce less wear when reciprocated against cartilage because of an increase in articular contact area, no trend between implant Young's modulus and wear was observed in the study presented in Chapter 3. PEEK produced significantly more wear than stainless steel, titanium, and UHMWPE, seemingly independently of stiffness or surface roughness average measurements, which were in the middle of the pack and the lowest, respectively. The data suggest that another property of PEEK, perhaps involving microscopic surface asperities or its chemical composition, led to the disproportionate damage that was observed. A detailed examination of PEEK's chemical composition in relation to its mechanical properties including wettability tests, micro-scale friction tests, and the effect of implant manufacturing methods are necessary to explain the mechanisms that caused the severe damage.

Chapter 3 concludes that between 0.69GPa and 200GPa, Young's modulus does not have an effect on cartilage wear in the context of hemiarthroplasty. However, an examination of much more compliant implant materials, such as hydrogels and Bionate, should be undertaken to determine whether stiffness will bear on wear outside of the range tested by this study.

5.4 The Effect of Implant Stiffness Contact Geometry and Stiffness on Cartilage Contact Mechanics: A Finite Element Study

A two-dimensional finite element model was constructed to identify stress levels and to compute the contact area of all of the implant geometries and materials investigated by this work. The decrease in stresses as implant model radius of curvature increased shown by the finite element simulation accords with the reduction in average volumetric wear

presented in Chapter 2, though stress levels decreased consistently as radius of curvature increased for all implant geometries, which supports the appearance of a stress threshold level.

The stress levels (which were shown to be nearly identical among all implant model materials) and the *in vitro* wear results presented in Chapter 3 also agreed. This supports the conclusion that within the span of moduli investigated, that Young's modulus does not have the prevailing effect on wear.

Finite element studies which examine materials with moduli approaching that of cartilage may reveal a stiffness-stress relationship, and should be undertaken to supplement our understanding. Additionally, a more complex, three dimensional finite element model may offer more insight, though it would be more computationally expensive.

5.5 Conclusion

The studies presented in this thesis provide a broad account of early *in vitro* cartilage wear, and present some novel insights on a relatively new field of study. While still at the level of basic science, the results may act as a starting point to improve the design of hemiarthroplasty implants so that they have more clinical applicability and success.

Appendices

Appendix A- Glossary

Abrasion	The process of damaging or wearing by friction.
Adhesion	The tendency of dissimilar particles of surfaces to cling to one another. The process of sticking due to mechanical or chemical surfaces.
Anisotropy	The directional dependence of material properties.
Arthroplasty	A surgical procedure which restores joint function.
Asperity	A rough edge on a surface; a local surface defect.
Excision	Surgical removal or resection.
Explant	A living cell, tissue, or organ that has been excised from the body.
Extension	The motion which moves two segments of the body apart.
Fibrillation	Degenerative changes marked by cartilage softening and development of vertical clefts between cartilage cells. Early sign of osteoarthritis.
Flexion	The motion of bringing two segments of the body closer together.
Hemiarthroplasty	A surgical procedure which restores joint function by replacing one articulating surface while leaving the others intact.
In situ	Latin: on site; a process or experiment conducted within the operating conditions of the components being examined.
In vitro	Latin: In glass; a process or experiment conducted outside of a living organism.
In vivo	Latin: Within the living; a process or experiment conducted in a living organism.
Lateral	In the direction away from the midline of the body.
Medial	In the direction towards the midline of the body.
Multiphasic	Consisting of many material phases or stages.
Osteoarthritis	Degeneration of articular cartilage which results in adaptive bone stiffening

	and reduces joint functionality.
Permeability	The resistance of fluid flow through a medium or material.
Spalling	Breaking off in fragments as a result of corrosion, weathering, impact, or cavitation.
Stiffness	The rigidity of an object; the extent to which it resists deformation in response to an applied force.
Tribology	The study of interacting surfaces in relative motion.
Wear	Damage or erosion by friction.

Appendix B- The Effect of Freezing on the Mechanical Properties of Articular Cartilage

The objective of this study was to compare the tribological properties of fresh and frozen articular cartilage to establish standards for specimen preparation. Cylindrical plugs of cartilage were harvested from fresh bovine stifle joints within 12 hours of death in a similar process to that described in Chapter 2 and Chapter 3, except that specimens were not frozen.

Specimens (N=6) were worn against spherically-tipped, 4.7 mm radius stainless steel pins using a reciprocating pin-on-disk tribometer at a rate of 1.4 Hz and a displacement of 152 meters under a constant load of 27.5 N . After testing, the specimens were stained with India ink. The stained cartilage plugs were photographed using a Chemi Genius 2 Bio Imaging System (Syngene, Cambridge, United Kingdom) under the following settings:

- Upper white on.
- White light box down.
- 1.31 m pixel, no filter.
- Exposure time: 8ms
- Iris= 1.2
- Zoom= 74.9
- Focus=104

Photos of the stained specimens were exported and thresholded using Fiji (ImageJ). The wear track was outlined manually to select a region of interest. These measurements were repeated three times and averaged to reduce error. The image was thresholded using the Isodata setting, and the threshold level was recorded for each image. Once all images were been individually thresholded, the mean threshold level was calculated, then applied to all of the images. The number of pixels darker than the threshold level in each image was converted to an area. Wear was assessed by normalizing this damaged area over the area of the total wear track for each image. This process was repeated for the frozen specimens, prepared in the ways described in Chapters 2 and 3. The average percent area damaged is shown in Figure A-1.

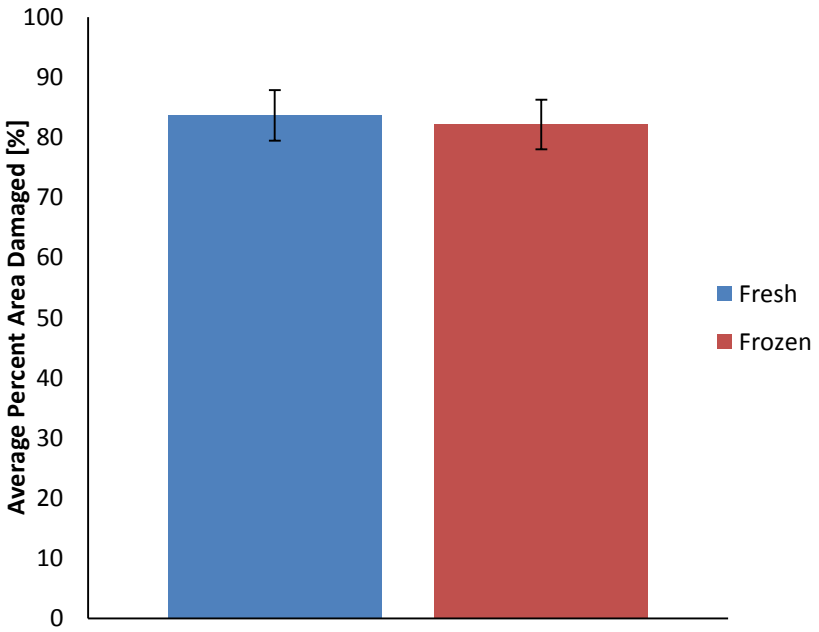

Figure A-1 *Percent area damage for fresh and frozen cartilage specimens.*

All specimens showed significant marked wear damage; however, no significant difference (p=0.858) was observed among the surface damage inflicted upon the fresh and frozen specimens. The mean surface area damaged was 83.65 % for fresh specimens and 82.15 % for frozen (STD=1.06 %).Based on the results of this study, frozen specimens, which are more easily accessible than their fresh counterparts, seem reasonable for use in wear studies.

Appendix C- Volumetric Wear of a Hemiarthroplasty Implant Roughness Grade Material

Table A-1 shows the surface roughness measurements taken using the Tencor P10 surface profilometer (Santa Clara, CA, USA) alongside the resultant volumetric wear after 10000 cycles on the tribometer. These results are depicted graphically in Figure A-2.

Table A-1 *Surface roughness measurements and volumetric wear for implant materials*

	Roughness Average [µm]	**Average Volumetric Wear [mm^3]**
Si_3N_4	0.02	2.1255
PEEK	1.27955	8.592675
HDPE	1.8092	5.111625
Ti	1.8639	4.2502
SS	1.95985	3.6219125
UHMWPE	2.08505	4.5912

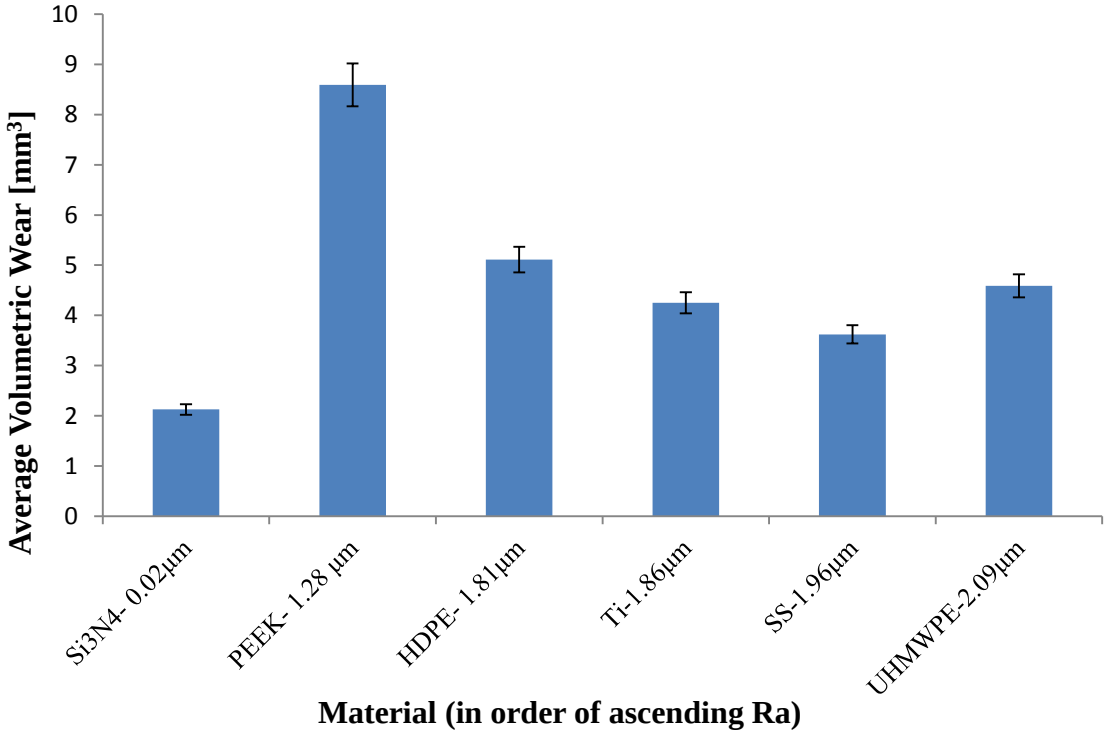

Figure A-2 *Volumetric wear for various materials, in order of ascending surface roughness average measurement.*

Appendix D- The Time-Dependence of Cartilage Wear

Figure A-3 shows the volumetric wear of cartilage specimens (n=6) worn with silicon nitride pins with 20 nm surface roughness average measurements as a function of number of cycles. Wear was simulated on a pin-on-plate tribometer under a constant load of 27.5 N, at a frequency of 1.2 Hz, and 5 mm stroke length. Wear was assessed in the ways described in Chapters 2 and 3, with measurements taken at each interval. Before scanning, specimens were allowed to reabsorb fluid until an additional, statically loaded sample reabsorbed fluid so that cartilage deformation was not mistaken for wear.

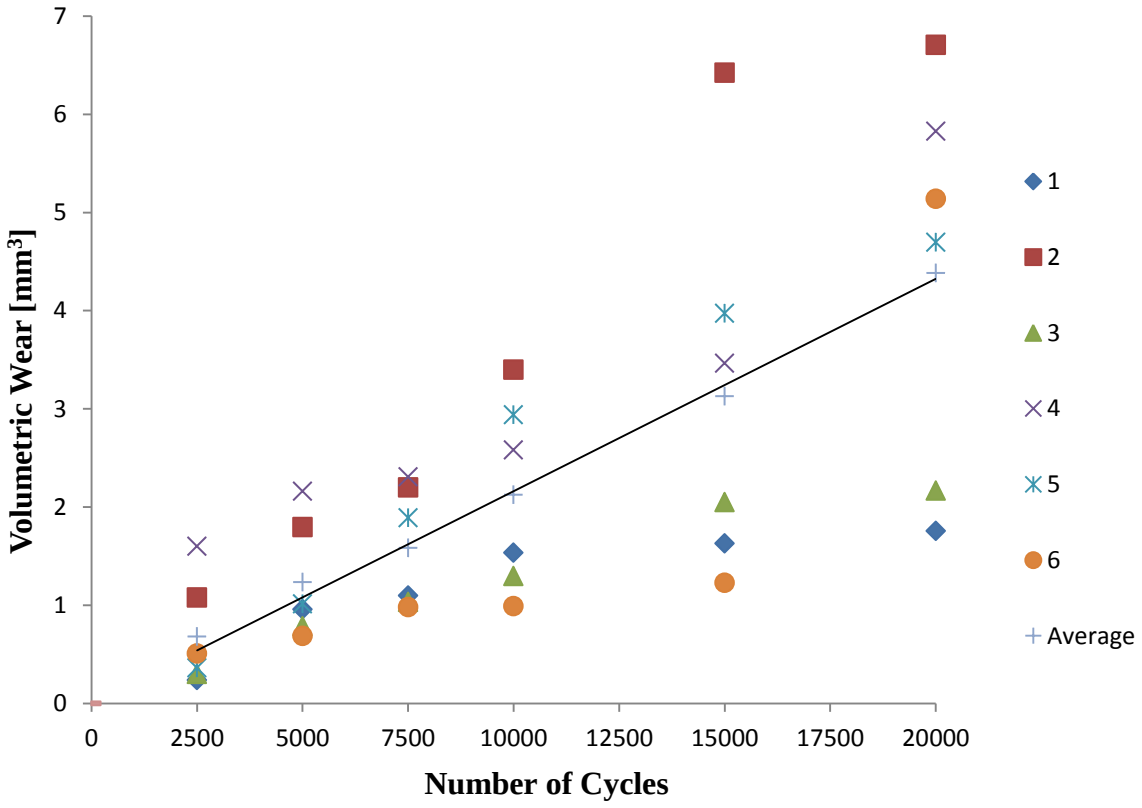

Figure A-3 *Volumetric wear as a function of number of reciprocation cycles.*

A fairly linear increase in wear was observed as the number of cycles increased, which supports the decision to select 10000 cycles as the total wear distance in the performed wear stuides. This enabled relatively quick wear testing, which enabled an increased sample size and prevented cartilage degeneration though testing.

Appendix E- Determination of Applied Load Level

In order to generate physiologically relevant stresses in the articular cartilage, a target maximum contact pressure level of 1.4 MPa was selected, which is within the physiological spectrum for intact joints. In order to determine the load level that would result in this contact pressure, the Hertzian theory of non-adhesive elastic contact was used. This model was used to approximately determine the applied force needed to achieve the prescribed maximum stress, which was then measured. Since the Hertzian model describes the interaction of non-conforming surfaces, the contact pressure was manually measured to assure that it was within the clinical range for hemiarthroplasty for all materials and geometries investigated (Appendix F). In the calculations, the implant model used to benchmark load levels was the 4.7mm tip stainless steel pin. The Hertzian model gives circular contact radius, *a*, as:

$$a = K_a \sqrt[3]{F}$$

Equation 1: *Hertzian Contact Radius*

$$\text{where } K_a = \left[\frac{3}{8} \frac{(1-\nu_1^2)/E_1 + (1-\nu_2^2)/E_2}{(1/d_1)+(1/d_2)} \right]^{1/3}$$

F = applied force

ν_1, ν_2 = Poisson's ratios for spheres 1 and 2

E_1, E_2 = elastic modulii for spheres 1 and 2

d_1, d_2 = diameters of spheres 1 and 2

The model also gives the maximum contact pressure, p_{max}, which occurs at the centre of the point of contact between two curved surfaces, which is calculated as:

$$p_{\max} = \frac{3F}{2\pi a^2}$$

Equation 2: *Maximum Hertzian Contact Pressure*

Therefore, with a known maximum contact pressure, we can calculate the required applied force, F. Table A-2 shows the variables used to determine the applied force necessary to reach the prescribed maximum contact pressure.

***Table A-2** Variables used in Hertizian Contact Stress Calculation*

	Stainless Steel	**Cartilage (in equilibrium)**
E	200	0.0001
ν	0.28	0.4
r [mm]	4.70	0 (for a flat plate)

This resulted in the 27.5 N load that was used in all testing scenarios.

Appendix F- Comparison of Clinical Contact Stresses and Contact Stresses of all Investigated Implant Models

Tables A-3 and A-4 show measured contact stresses for each implant geometry and clinical contact stresses for various hemiarthroplasty procedures respectively. All of the contact stress levels measured for the implants investigated fall within the clinically relevant ranges.

Table A-3 *Average contact stresses for implant models. Contact stresses were computed by dividing the applied force by the measured contact area from the pressure-sensitive Fuji Film and the casting technique, and the direct measurements taken from the FEA results*

	Average Contact Stress [MPa]		
ROC[mm]	Fuji Film (normalized)	Cast (normalized)	FEA (from software)
4.7	2.843846949	2.774974773	3.158167855
5.1	2.509124088	2.624045802	2.719169469
7.25	2.028023599	2.312867956	2.284414155
9.35	1.579551982	1.476906552	1.810100709
11.7	1.42118863	1.310147689	1.534101688

Table A-4 *Clinically Measured Contact Stresses for Various Hemiarthroplasty Procedures*

Joint	**Pre-Op Contact Stress [MPa]**	**Post-op Contact Stress [MPa]**
Shoulder (humeral head replacement against glenoid)	0.298 (Petragliaet al., 2014)	2.28 (Petragliaet al., 2014)
Elbow (radial head replacement against capitellum)	2.3 (Sahuet al., 2014)	5.4 (Sahuet al., 2014)
Hip (Femoral head replacement against)	1.67 (Gendaet al.,2001)	18 (Genda et al., 2001)

Appendix G- Cartilage Creep Measurements for all Testing Configurations implant models

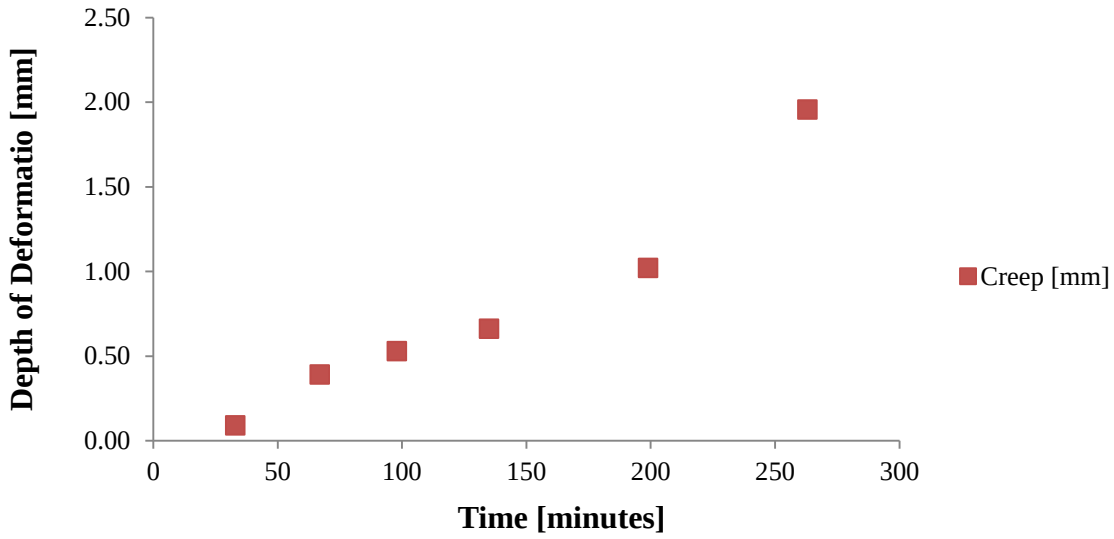

Figure A-4 *Penetration depth of a 4.70mm radius of curvature hemispherical tip pin under a constant, static load of 27.5N as a function of time.*

Table A-5 *Penetration depth and recovery time for cartilage loaded statically under 27.5 N with various implant geometries.*

	4.70mm	**5.10mm**	**7.25mm**	**9.35mm**	**11.7mm**
Time Until LS recovered [s]	123	123	122	119	119
Penetration depth at 139 minutes [mm]	1.24	1.51	0.81	1.14	1.51

Appendix H- MeshLab Mesh Registration, VTK Inter-Mesh Distance Algorithm, and MATLAB Volume Calculation Protocols

The pre- and post-wear scans of each sample were imported at .ply files to MeshLab. In the "Align" feature tab, the position of the pre-wear scan was fixed by selecting "Glue Here Mesh." Then, after selecting the post-wear scan, the "Point Based Gluing" option was used. This setting allows the user to select landmarks on the two surfaces to merge meshes. Four landmarks were selected, and the merging was completed by "Processing" the translation. This process was repeated until the average mesh alignment error was under five percent. The merged meshes were exported by flattening the visible layers, and saving a single file in .Ply format.

The merged mesh was then opened in ParaView (Kitware, Inc, New York, USA), then the 'Connectivity' filter was used to separate the worn and unworn surfaces. The meshes were then thresholded, and saved as binary .vtk files. The models were both opened in 3D Slicer, wherein the Model-to-Model distance extension was used to compute the signed distance between the two surfaces. A model that shows the distance between surfaces was generated and exported in binary format in the form of a colour-contour map, and opened in ParaView. The 'point data to cell data' filter was applied to model, which was then exported, this time in ASCII format.

The matlab .m file shown in Figure A-5 was then used to compute volume between the two surfaces, which corresponds to the volumetric wear.

```
function [postive_volumesnegative_volumes] = parse_surface_results(input_file)
% This program parses an input VTK surface and extracts the points and
% polys

% initialize incase they don't get filled;
Dist_data=[];

%Read in source surface info
fid=fopen(input_file,'r');

compare1=false;
compare2=false;

DIST=false;
```

```
while 1
        tline=fgetl(fid);
        compare1 = strncmpi(tline,'POINTS',6);
   compare2 = strncmpi(tline,'POLYGONS',8);
   compare3 = strncmpi(tline,'CELLS',5);
   DIST = strncmpi(tline,'SCALARS Distance',16);
   DIST2 = strncmpi(tline,'SCALARS Signed',14);

        if tline==-1
            break
   end

        if (compare1==true)
        npoints=sscanf(tline,'%*s %i %*s',[1]);
        fseek(fid,0,'cof');
        points=fscanf(fid,'%g',[3,npoints]);
        end

        if (compare2==true)
                npolys=sscanf(tline,'%*s %i %*s',[1]);
fseek(fid,0,'cof');
                polys=fscanf(fid,'%*i %i %i %i',[3,npolys]);
   end

   if (compare3==true)
                npolys=sscanf(tline,'%*s %i %*s',[1]);
fseek(fid,0,'cof');
                polys=fscanf(fid,'%*i %i %i %i',[3,npolys]);
   end

   if (DIST==true)||(DIST2==true)
fseek(fid,0,'cof');
      temp=fgetl(fid);
Dist_data=fscanf(fid,'%f');
   end

end
fclose(fid);
points=points';
polys=polys';
X=(points(polys(:,1)+1,1)+points(polys(:,2)+1,1)+points(polys(:,3)+1,1))/3;
Y=(points(polys(:,1)+1,2)+points(polys(:,2)+1,2)+points(polys(:,3)+1,2))/3;
Z=(points(polys(:,1)+1,3)+points(polys(:,2)+1,3)+points(polys(:,3)+1,3))/3;
centroids=[X Y Z];
V_1_X=points(polys(:,2)+1,1)-points(polys(:,1)+1,1);
V_1_Y=points(polys(:,2)+1,2)-points(polys(:,1)+1,2);
V_1_Z=points(polys(:,2)+1,3)-points(polys(:,1)+1,3);
V_1=[V_1_X V_1_Y V_1_Z];
V_2_X=points(polys(:,3)+1,1)-points(polys(:,1)+1,1);
V_2_Y=points(polys(:,3)+1,2)-points(polys(:,1)+1,2);
V_2_Z=points(polys(:,3)+1,3)-points(polys(:,1)+1,3);
```

```
V_2=[V_2_X V_2_Y V_2_Z];

NORM=cross(V_1,V_2,2);

areas=((NORM(:,1).*NORM(:,1)+NORM(:,2).*NORM(:,2)+NORM(:,3).*NORM(:,3)).^0.5)/2;
normals=NORM./[((NORM(:,1).*NORM(:,1)+NORM(:,2).*NORM(:,2)+NORM(:,3).*NORM(:,3
)).^0.5) ((NORM(:,1).*NORM(:,1)+NORM(:,2).*NORM(:,2)+NORM(:,3).*NORM(:,3)).^0.5)
((NORM(:,1).*NORM(:,1)+NORM(:,2).*NORM(:,2)+NORM(:,3).*NORM(:,3)).^0.5)];
volumes=Dist_data.*areas;
postive_volumes=sum(volumes(find(volumes>0)));
negative_volumes=sum(volumes(find(volumes<0)));
```

Figure A-5*.m file to compute volume between worn and unworn surface meshes.*

Appendix I- Contact Area Measurements for Various Measurement Techniques

Table A-6 *Contact area measurements for various techniques*

	Average Contact Area [mm^2]		
ROC [mm]	Fuji Film	Casting Technique	FEA
4.70	9.67	9.91	8.70
5.10	10.96	10.48	10.11
7.25	13.56	11.89	12.03
9.35	17.41	18.62	15.19
11.7	19.35	20.99	17.92

ALANA KHAYAT

EDUCATION

The University of Western Ontario, London, Ontario
MESc Biomedical Engineering, Biomechanics **2013- 2015**
Thesis: Effect of Hemiarthroplasty Implant Contact Geometry and Material on Early Cartilage Wear

The University of Western Ontario, London, Ontario
BESc, Mechanical Engineering **2008-2013**

The University of Western Ontario, London, Ontario
BA, Philosophy **2008-2013**
Areas of Concentration: philosophy of science and philosophy of language

AWARDS

First Prize in the Mechanical and Materials Engineering Design Day Competition, UWO **2013**

RESEARCH EXPERIENCE

Roth McFarlane Hand and Upper Limb Centre, St Joseph's Healthcare, London, Ontario
Research Assistant **Sept 2013 – present**

- Developed and validated a protocol to assess *in vitro* wear on articular cartilage
- Established standards for the preparation of bovine articular cartilage samples
- Evaluated the effects of implant geometry and material on cartilage wear concurrently with ABAQUS finite element analyses

TEACHING EXPERIENCE

The University of Western Ontario, London, Ontario
Teaching Assistant- Business for Engineers **Sept 2014-April 2015**
Proctored and graded examinations; marked assignments **Sept 2013-April 2014**

Teaching Assistant- Biomechanics of the Musculoskeletal System **Jan 2015-April 2015**
Coordinated tutorial sessions; prepared and presented lectures; proctored and graded examinations; marked assignments **Jan 2014-April 2014**

Teaching Assistant- Product Design and Development **Sept 2014-Dec 2014**

Proctored and graded examinations; marked assignments

The University of Western Ontario, London, Ontario
Teacher- Western Engineering Summer Academy **July 2014-Aug 2014**
Prepared and presented lecture material; planned and facilitated an interactive laboratory exercise to demonstrate the principles of the lectures

Teaching Assistant- First Year Design and Innovation Studio **1/1/2014**
Conducted studio sessions to guide and advise students' design decisions; evaluated presentations, assignments, reports, and comprehensive design projects

PROFESSIONALEXPERIENCE

Point Pelee National Park, Leamington, Ontario
Interpreter **May 2012 – Sept 2012**

- Researched, planned, and guided hikes and canoe tours in French and English
- Produced and published interpretive manuals
- Prepared and presented demonstrations with live animals

Outland Reforestation, Toronto, Ontario
Tree Planter **Summer: 2010, 2011**

- Planted seedlings in rough terrain for upwards of ten hours a day in remote areas
- Managed vast pieces of land, adhered to quality standards for spacing, tree quality, and microsite selection

Exact Oil, Harrow Ontario
Translation Group Leader **Oct 2006-Feb 2007**

- Translated all product information including safety information from English to French
- Chaired group meetings to establish standards for translated documents
- Edited and standardized language in documents translated by other translators before submission

Red Ball Dock Systems, Leamington, ON
Administrative Assistant **June 2004-Sept 2006**

- Assisted in general office administration and management

CONFERENCE PRESENTATIONS

"The Effect of Hemiarthroplasty Contact Geometry on Early In-Vitro Cartilage Wear"
Podium presentation at the 2015 Annual Meeting of the Canadian Orthopaedic Research Society

"The Effect of Hemiarthroplasty Contact Geometry on Early In-Vitro Cartilage Wear"
Poster presented at the 2015 Annual Meeting of the Canadian Orthopaedic Association/ Canadian Orthopaedic Research Society

"The Effect of Pin Geometry on Early Cartilage Wear in Linear Reciprocal Sliding"
Poster presented at the 2015 Annual Meeting of the Orthopaedic Research Society

LANGUAGES

English- Native language
French- Fluent speaker and proficient in reading and writing, with a Certificate of Bilingual Studies in French Immersion
Arabic- Fluent speaker

TECHNICAL SKILLS

Proficient in:

- SolidWorks
- SolidWorks Simulation
- AutoCAD
- Microsoft Excel
- MathCad
- MeshLab

Knowledge of:

- MATLAB
- ParaView
- FIJI
- 3D Slicer
- Autodesk Inventor

DESIGN PROJECTS

The University of Western Ontario, London, Ontario
Wood Burning Stove **Sept 2012-April 2013**

- Participated in the conception, design, modeling, construction, and testing of an innovative, environmentally-friendly, and fully-validated wood burning stove and air circulation system
- Won first prize in the Mechanical and Materials Engineering Design Day competition
- Created CAD drawings for manufacturing using Autodesk Inventor, and 3D CAD models using SolidWorks
- Optimized design parameters and dimensions using SolidWorks Computational Fluid Dynamics and Thermal Analysis
- Bended, welded, and assembled laser-cut steel to construct the stove

- Empirically tested the stove for parameters including efficiency, thus validating the model

The University of Western Ontario, London, Ontario
Active Magnetic Therapeutic Insole for Relief of Foot Pain Associated with Diabetes **Jan 2014-April 2014**

- Participated in the design, modeling, construction, and testing of a discrete insole for the treatment of foot pain associated with diabetic peripheral neuropathy
- Produced standard-size insole that generated magnetic field sufficient to distort pain signals in the foot
- Utilized a piezoelectric force detection system, an Arduino microcontroller, and an electromagnetic drive circuit to initiate the therapeutic magnetic field

The University of Western Ontario, London, Ontario
Beer Keg Trolley **Jan 2010-April 2010**

- Designed an ergonomic, collapsible trolley to transport beer kegs with the aim of injury prevention in the food-service industry
- Modeled the self-latching handle and base system in SolidWorks
- Performed stress analysis using SolidWorks Simulation finite element analysis

VOLUNTEERING

Moksha Yoga London Downtown, London, ON
Energy Exchange Program Member **Sept 2013 – present**
Sold memberships; signed clients in; cleaned hot practice room; stocked merchandise; helped organize community events and activities

Ten Thousand Villages, Leamington, Ontario
Volunteer **June 2005 – August 2008**
Tended to customers; placed product orders; stocked and organized merchandise while advocating for fair trade

Frontier College
English as a Second Language Tutor **Sept 2007 – July 2008**
Tutored students new to Canada by doing homework, practicing conversational English, and engaging in social activities